ilmedia

TECHNISCHE UNIVERSITÄT ILMENAU

Zhang, Zhiyong; Sattel, Thomas; Zhu, Yujie; Li, Xuan; Dong, Yawei; Rui, Xiaoting:

Mechanism and characteristics of global varying compliance parametric resonances in a ball bearing

Mechanism and Characteristics of Global Varying Compliance Parametric Resonances in a Ball Bearing

Zhiyong Zhang [1,2,3,4,*], Thomas Sattel [2], Yujie Zhu [1], Xuan Li [1], Yawei Dong [1] and Xiaoting Rui [3]

[1] School of Science, Nanjing University of Science and Technology, Nanjing 210094, China; yujiezhu@njust.edu.cn (Y.Z.); lixuan1995@njust.edu.cn (X.L.); yaweidong@njust.edu.cn (Y.D.)

[2] Mechatronics Group, Department of Mechanical Engineering, Technische Universität Ilmenau, 98684 Ilmenau, Germany; thomas.sattel@tu-ilmenau.de

[3] Institute of Launch Dynamics, Nanjing University of Science and Technology, Nanjing 210094, China; ruixt@163.net

[4] State Key Laboratory of Mechanical Behavior and System Safety of Traffic Engineering Structures, Shijiazhuang Tiedao University, Shijiazhuang 050043, China

* Correspondence: zhiyzhang@njust.edu.cn

Abstract: Varying compliance (VC) is an unavoidable form of parametric excitation in rolling bearings and can affect the stability and safety of the bearing and its supporting rotor system. To date, we have investigated VC primary resonance in ball bearings, and in this paper other parametric VC resonance types are addressed. For a classical ball bearing model with Hertzian contact and clearance nonlinearities between the rolling elements and raceway, the harmonic balance and alternating frequency/time domain (HB–AFT) method and Floquet theory are adopted to analyze the VC parametric resonances and their stabilities. It is found that the 1/2-order subharmonic resonances, 2-order superharmonic resonances, and various VC combination resonances, such as the 1-order and 2-order summed types, can be excited, thus resulting in period-1, period-2, period-4, period-8, period-35, quasi-period, and even chaotic VC motions in the system. Furthermore, the bifurcation and hysteresis characteristics of complex VC resonant responses are discussed, in which cyclic fold, period doubling, and the second Hopf bifurcation can occur. Finally, the global involution of VC resonances around bearing clearance-free operations (i.e., adjusting the bearing clearance to zero or one with low interference) are provided. The overall results extend the investigation of VC parametric resonance cases in rolling bearings.

Keywords: ball bearing; VC parametric vibration; subharmonic resonance; combination resonance; HB–AFT method; Floquet theory

1. Introduction

Faraday [1] previously recognized the phenomenon of parametric resonance when he studied the response frequency of surface waves in a fluid-filled cylinder with vertical excitations. Researchers have subsequently carried out extensive investigations of parametric resonances for various nonlinear vibration systems in the field of neutrino oscillations [2], quantum fields [3], ship dynamics [4], Brownian dynamics of water droplets [5], bubbles oscillating in water [6], micro-electro mechanical systems [7,8], and rotor dynamics [9,10]. Therefore, the topic of parametric resonance is a basic scientific problem in the field of nonlinear dynamics.

Rolling bearings are widely used in rotating machineries due to their advantages of lower friction compared to sliding bearings and ease with which they can be selected from a manufacturer's catalogue [11]. There are two major effects of a healthy rolling bearing on machine vibration [12,13]:

spring characteristics and the excitation force on the supported structure. In the dynamic design of the bearing-rotor system, the excitation characteristics of rolling bearings should be given adequate consideration. Varying compliance (VC) excitation is induced when rolling elements move along the bearing raceway with an external load, which results in time-varying bearing stiffness in the rotor system. Thus, VC excitation is an inevitable case of parametric excitation [9,14].

Sunnersjö [9] found that VC excitation can result in periodic and irregular non-periodic vibrations in cylindrical roller bearings using digital simulation and experiments. Fukata et al. [14] identified that VC vibration may exhibit subharmonic, quasi-periodic, chaotic, and beat motions at critical speeds, considering a two-degree-of-freedom ball bearing model with Hertzian contact nonlinearity. Mevel and Guyader [15,16] studied the routes to chaos in ball bearings and noted the chaos due to period doubling in the resonant speed range. Tomović [17] found that the VC vibration amplitude of rolling bearings is directly related to the bearing deflection in two specific boundary positions of the rolling elements, and a simplified rolling bearing model for description of VC vibrations was presented. Regarding VC hysteresis characteristics, Sankaravelu et al. [18] found a hysteretic amplitude–frequency response in ball bearing VC vibration using an early shooting method. Ghafari et al. [19] investigated the hysteresis behaviors using static bifurcation analysis and provided closed-form expressions of VC periodic solutions using the generalized averaging method. Based on Hertzian contact resonance [20,21], Zhang et al. [22–25] investigated the mechanism, influence, and suppression of VC resonant hysteresis in ball bearings. Theoretical and experimental results showed that the primary contact resonance exhibits soft spring behavior in the direction exerting constant force, and the coexistence of soft and hard spring characteristics in the direction with zero external force. In addition, Zhang et al. [26] noted a case of complex coupling VC resonance caused by the superposition of VC parametric primary resonance and 1:2 internal resonance. The above research is mainly focused on the primary VC resonant responses. However, it should be noted that a small parametric excitation may produce remarkable responses, even if the excitation frequency significantly differs from the linear natural frequencies of the system [27]. Other parametric resonance types may also exist in a parametric system, such as superharmonic, subharmonic, and combined cases.

Rapid, flexible, and automated development requires higher stability and safety characteristics in rotating machineries, which promotes the study of super- and subharmonic resonances, and their combinations, in rolling bearing-rotor systems. Tiwari et al. [28,29], Harsha et al. [30,31], and Bai et al. [32] presented the amplitude and stability of VC responses for a rolling bearing-rotor system in a large speed range; however, the mechanism of the resonant amplitude has been little addressed. Ehrich [33] observed high-order subharmonic vibration responses under low damping and strong nonlinearity conditions in high speed rotating machinery with asymmetric bearing supports, based on the numerical integration of a finite difference formulation. Yoshida et al. [34] showed the soft and hard hysteretic 1/2-order subharmonic resonances in different degrees of freedom of a ball bearing-rotor system using the multi-scale method. Although this study also found combination resonances between the 1/2-order subharmonic resonance intervals, this has not been analyzed in depth. Bai et al. [35] established a 6DOF nonlinear ball bearing-rotor model and found that the occurrence of 2-order subharmonic resonance is provoked by the coupling of Hertzian contact and internal clearance nonlinear factors of ball bearings. Wu et al. [36] noted that the subharmonic hysteretic resonance become significant and the resonance amplitude moved to lower frequencies as the assembly gap increased for an angular contact high-speed ball bearing system. However, these studies [33–36] relate to the case of external excitations from unbalanced rotors, for which a small excitation produces a large response only if the frequency of the external excitation is close to that of the linear natural frequency of the system, and it is essentially different from that of the parametric excitation system. Therefore, a global mechanism analysis of VC parametric resonances in rolling bearings is necessary.

Bearing clearance is a basic parameter of rolling bearings, and has a significant effect on bearing life, installation, and bearing stiffness [11,12]. Yammamoto [37] previously showed that the resonant frequency and amplitude can be reduced to some extent as the clearance adjusts. Oswald et al. [38]

noted that the bearing life declines gradually with positive clearance and rapidly with increasing negative clearance, and the life can be maximized for a small negative operating clearance. In the field of bearings, it is generally considered that adverse vibration and noise behaviors can be reduced by adjusting the ball bearings to zero clearance [39]. In particular, a clearance-free operation is usually desirable for precision or high-speed machinery, such as machine tools and turbines [11]. Therefore, the study of VC parametric resonances in clearance-free operations for rolling bearing systems is valuable.

The harmonic balance and alternating frequency/time domain (HB–AFT) method is an effective means to obtain the steady-state harmonic solutions of a general nonlinear system. It can be used to quickly obtain the frequency domain information of the nonlinear term for the harmonic balance process of the AFT discretization technology [40]. Kim et al. [41] and Guskov et al. [42] developed the generalized HB–AFT method to analyze the quasi-periodic response characteristics of multiple degrees-of-freedom and multi-frequency excitation systems. Zhang et al. [22] embedded continuation and Hsu's Floquet stability analysis technology into the HB–AFT method, which can automatically track the periodic response and bifurcation characteristics of nonlinear systems. Recently, Chen et al. [43] developed a harmonic balance method combined with the model incremental transfer matrix of the system, which is highly convenient for dealing with systems with multiple degrees-of-freedom.

The motivation of the present work is to provide a better understanding of the VC parametric resonances in a ball bearing. The mechanisms of various new cases of parametric resonances are provided mainly using the HB–AFT method with the Floquet theory, and their detailed response characteristics, such as time series, orbit, stability, and hysteresis, are investigated. The global amplitude–frequency responses around the bearing clearance-free operations are examined in detail and predicted.

2. Description of Ball Bearing VC Vibration

Considering the nonlinearities of VC parametric excitation, bearing clearance, and the Hertzian contact between the rolling elements and raceway, a classic two degrees-of-freedom ball bearing model is studied here. This model has been verified for qualitative and quantitative analysis of the response characteristics of radial VC motions in ball bearings [14–16,24], and the JIS6306 specification shown in Table 1 is adopted in this article.

Table 1. Specifications of JIS6306 ball bearing [22].

Item	Value
Contact stiffness C_b (N/m$^{3/2}$)	1.334×10^{10}
Ball diameter D_b (mm)	11.9062
Pitch diameter D_h (mm)	52.0
Number of balls N_b	8
Equivalent mass m (kg)	20
Damping factor c (Ns/m)	200
Radial load W (N)	196

As shown in Figure 1, the instant angular location of the ith ball is denoted as:

$$\theta_i = 2\pi(i-1)/N_b + \Omega t \tag{1}$$

with ball passing frequency (i.e., the cage angular velocity) of:

$$\Omega = \omega_S(1 - D_b/D_h)/2 \tag{2}$$

Then, the contact deformation between the ith ball and bearing raceways is expressed as:

$$\delta_i = x\cos\theta_i + y\sin\theta_i - \delta_0 \tag{3}$$

where ω_s and $2\delta_0$ denote the rotor shaft speed and the radial internal bearing clearance, respectively.

Assuming only Hertzian contact deformations are considered, the nonlinear restoring forces F_x and F_y are:

$$\begin{bmatrix} F_x \\ F_y \end{bmatrix} = C_b \sum_{i=1}^{N_b} (\delta_i G[\delta_i])^{1.5} \begin{bmatrix} \cos\theta_i \\ \sin\theta_i \end{bmatrix} \tag{4}$$

where $G[\cdot]$ is a Heaviside function, taking 1 if $\delta_i \geq 0$ represents the condition of contact, or else taking 0, which denotes the contact loss between the rolling element and raceway.

The VC motion of a rigid Jeffcott rotor-ball bearing system can be expressed as:

$$m\begin{bmatrix} \ddot{x} \\ \ddot{y} \end{bmatrix} + c\begin{bmatrix} \dot{x} \\ \dot{y} \end{bmatrix} + \begin{bmatrix} F_x \\ F_y \end{bmatrix} = \begin{bmatrix} W \\ 0 \end{bmatrix} \tag{5}$$

Due to the Hertzian contact deformation relationship, the system has hard spring characteristics [44–46]. The approximate linearized static stiffness of System (5) in the direction of static load W_s can be expressed as [46]:

$$k_{W_s} = \frac{dW_s}{d\delta_{W_s}} = \frac{1.5W_s}{\delta_{W_s}} \tag{6}$$

where δ_{W_s} denotes the total deformation along the direction of W_s.

Equation (6) is clearly not applicable for the estimation of the dynamic stiffness of a ball bearing system during operation. The dynamic stiffness characteristics of rolling bearings have a significant impact on the nonlinear response characteristics of their supporting systems [12,22,26]. According to the restoring forces of Equation (4), the radial linearized dynamic stiffness of the system can be approximated as [15]:

$$\begin{bmatrix} k_{xx}(t) \\ k_{yy}(t) \end{bmatrix} = \begin{bmatrix} \partial F_x(t)/\partial x \\ \partial F_y(t)/\partial y \end{bmatrix} \tag{7}$$

Then, the dynamic resonant frequencies of the system can be expressed as:

$$\begin{bmatrix} \omega_{xx}(t) \\ \omega_{yy}(t) \end{bmatrix} = \begin{bmatrix} \sqrt{k_{xx}(t)/m} \\ \sqrt{k_{yy}(t)/m} \end{bmatrix} \tag{8}$$

and the equivalent resonant frequencies ω_{x0}, ω_{y0} can be estimated from the arithmetic mean of Equation (8) [22].

The VC parametric excitation frequency occurs due to the ball passage frequency, which can be expressed as:

$$\Omega_{VC} = N_b \cdot \Omega \tag{9}$$

Many cases of resonance might exist in a parametric excitation system with many degrees-of-freedom [27,47,48], and the conditions of possible excited VC parametric primary, subharmonic, and superharmonic resonances are:

$$\Omega_{VC} \approx \left\{ n \cdot \omega_{xx}, \ m \cdot \omega_{yy}, \ 1/n \cdot \omega_{xx}, \ 1/m \cdot \omega_{yy} \right\} \tag{10}$$

where the VC parametric primary resonance can occur when $n(m) = 1$; $1/h$-order subharmonic resonances can emerge when $n(m) = h$; the h-order superharmonic resonance may be excited when $n(m) = 1/h$. In addition, VC parametric combination resonance might occur in (but is not limited to) the following conditions:

$$\Omega_{VC} \approx n \cdot \omega_{xx} \pm m \cdot \omega_{yy} \pm 1/j \cdot \omega_{xx} \pm 1/k \cdot \omega_{yy} \tag{11}$$

and "≈" denotes an approximation to the value in Equations (10) and (11); *h*, *m*, *n*, *j* and *k* are positive integers, where $h \neq 1$.

Moreover, due to the possible hysteresis characteristics of the dynamic stiffness of a nonlinear system [25,49], multiple resonance cases might coexist.
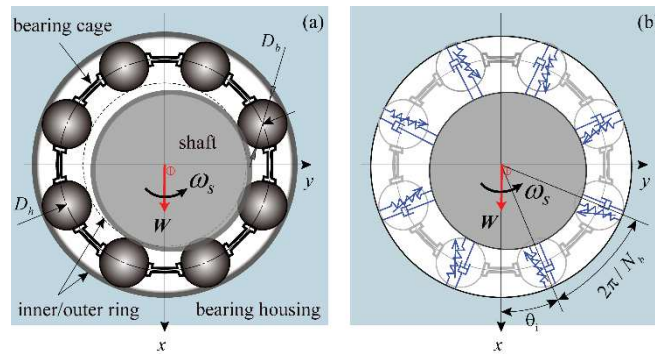

Figure 1. Schematic diagram of (**a**) the ball bearing system, and (**b**) its two degrees-of-freedom spring model.

3. Methodology

For a periodically excited nonlinear vibration system, a periodic motion is called the period-*M* motion if the period of the response is *M* times the excited period, and the *M*-order subharmonic resonance interval must contain period-*M* solutions. The process of deriving the VC period-*M* solution and the stability analysis for the studied System (5) is given below.

3.1. HB–AFT Method for Obtaining VC Period-M Solution

To improve the accuracy and efficiency of obtaining the VC period-*M* solution, one can introduce a dimensionless displacement $\boldsymbol{X} = [X, Y]^{\mathrm{T}} = [x/\delta_0, y/\delta_0]^{\mathrm{T}}$, and dimensionless time $\tau = N_b \cdot \Omega \cdot t / M$; then, Equation (5) can be expressed as:

$$\boldsymbol{X}''(\tau) = \boldsymbol{F}(\boldsymbol{X}(\tau), \boldsymbol{X}'(\tau), \lambda) \tag{12}$$

Here, let the control parameter $\lambda = \Omega$ for tracing the amplitude–frequency response curves, and for System (12) the period T_{VC} of the VC period-*M* solution is 2π. Then, $\boldsymbol{X}(\tau)$ and $\boldsymbol{F}(\cdot)$ can be expressed as:

$$\begin{bmatrix} X \\ F \end{bmatrix} = \begin{bmatrix} a_0 \\ c_0 \end{bmatrix} + \sum_{k=1}^{K} [\begin{bmatrix} a_k \\ c_k \end{bmatrix} \cos(k\tau) - \begin{bmatrix} b_k \\ d_k \end{bmatrix} \sin(k\tau)] \tag{13}$$

According to the process of harmonic balance, insert Equation (13) into Equation (12) and obtain the following $4K + 2$ algebraic relationships:

$$g(\boldsymbol{P}, \boldsymbol{Q}, \lambda) = 0 \tag{14}$$

where the harmonic coefficients of $\boldsymbol{X}(\tau)$ and $\boldsymbol{F}(\cdot)$ are:

$$\begin{bmatrix} P \\ Q \end{bmatrix}^{\mathrm{T}} = \begin{bmatrix} a_0, \ a_1, \ b_1, \ a_2, \ b_2, \ \ldots, \ a_K, \ b_K \\ c_0, \ c_1, \ d_1, \ c_2, \ d_2, \ \ldots, \ c_K, \ d_K \end{bmatrix}^{\mathrm{T}} \tag{15}$$

To obtain $\boldsymbol{P}$ from Equation (14), it should first formulate $\boldsymbol{Q}$ by $\boldsymbol{P}$, because Equation (14) contains $8K + 4$ unknown harmonic coefficients of $\boldsymbol{P}$ and $\boldsymbol{Q}$, and this process can be completed by the following AFT technology.

The discrete sample of $X(\tau)$ is given by the inverse discrete Fourier transform as:

$$X(n) = \text{Real}\{\sum_{k=0}^{K} P_k e^{i(2\pi kn/N)}\} \tag{16}$$

and the discrete time domain sample of Equation (12) is:

$$F(n) = F(X(n), X'(n), \lambda) \tag{17}$$

Then, by discrete Fourier transform, Q can be expressed as:

$$Q_k = \frac{\phi}{N} \sum_{n=0}^{N-1} F(n) \, e^{i(-2\pi kn/N)} \tag{18}$$

Herein, $P_k = a_k + i \, b_k$; $Q_k = c_k + i \, d_k$; N is the numbers of samplings in the time domain, and $n = 0, \ldots, N-1$; $\phi = 1$ if $n = 0$, or else $\phi = 2$.

At this moment, Q is formulated by P as shown in Equation (18). Taking P as an unknown variable, one can obtain the harmonic solution of $X(\tau)$ by solving the nonlinear algebraic Equation (14). In order to avoid the singular case at the turning point and track P automatically, the arc-length continuation is introduced by transforming Equation (14) into following form [22]:

$$\begin{cases} \frac{dg}{dP}\frac{dP}{ds} + \frac{dg}{d\lambda}\frac{d\lambda}{ds} = 0 \\ \frac{dP}{ds}\frac{dP^T}{ds} + \left(\frac{d\lambda}{ds}\right)^2 = 1 \end{cases} \tag{19}$$

where s denotes the arc-length parameter of curve $(P(s), \lambda(s))$.

Finally, Equation (19) can be solved by the predictor–corrector procedure [50], where the value of the initial condition $(P(s_0), \lambda(s_0)) = (P, \lambda)_0$ is searched for using the HB–AFT process above.

3.2. Floquet Stability Analysis of VC Period-M Solution

In the following section, the detailed process of stability analysis for VC period-M solution $U^*(\tau)$ obtained in Section 3.1 will be given by using Floquet stability theory [51].

Introducing $U = [X, X', Y, Y']^T = [X_1, X_2, X_3, X_4]^T$, transform System (12) into:

$$U'(\tau) = H(\tau, U(\tau)) = \begin{bmatrix} X_2 \\ \frac{1}{m}\left(\frac{W - F_x}{\delta_0 \Omega_M^2} - \frac{cX_2}{\Omega_M}\right) \\ X_4 \\ -\frac{1}{m}\left(\frac{F_y}{\delta_0 \Omega_M^2} + \frac{cX_4}{\Omega_M}\right) \end{bmatrix} \tag{20}$$

where $\Omega_M = N_b \cdot \Omega / M$.

For Equation (20), superpose ΔU to perturb the VC period-M solution $U^*(\tau)$, i.e.,

$$(U^*(\tau) + \Delta U)' = H(\tau, U^*(\tau) + \Delta U) \tag{21}$$

and retain only linear terms in the disturbance as:

$$\Delta U' = \partial H(\tau, U^*(\tau))/\partial U^*(\tau) \cdot \Delta U \tag{22}$$

Then, the local linear stability of $U^*(\tau)$ can be provided by the stability information of Equation (22). As $U^*(\tau)$ is a period-M solution of the System (20), $\partial H(\tau, U^*(\tau))/\partial U^*(\tau)$ is also a periodic variable matrix, and the stability of the VC period-M solution $U^*(\tau)$ can be determined by the eigenvalues of the Floquet monodromy matrix of Equation (22).

The Hsu method [22] is used to calculate the Floquet multiplier λ_m and, according to the three means of λ_m passing the unit circle of a complex plane, the period-*M* solution $U^*(\tau)$ can lose stability as follows [51]:

- A transcritical, symmetry-breaking, or cyclic-fold bifurcation may originate when the leading multiplier crosses through the unit circle at +1. Herein, the cyclic-fold bifurcation emerges only at the turning point of a solution branch.
- A period-doubling bifurcation occurs when the leading multiplier crosses the unit circle at −1.
- A secondary Hopf bifurcation occurs when a complex pair of multipliers moves out of the unit circle.

4. Results

4.1. The VC 2-Order Superharmonc Resonance, 1/2-Order Subharmonic Resonance and the Case of $\omega_{x0} + \omega_{y0}$ = Ω_{vc} Combination Resonance

For $\delta_0 = 1.5$ µm, Figure 2 shows the VC period-1 and period-2 solution branches traced by the HB–AFT method with arc-length continuation. Predicting from Equations (8) and (9), the equivalent resonant frequencies of the two degrees of freedom of System (5) are about $\omega_{x0} = 1908.14$ rad/s and $\omega_{y0} = 1297.36$ rad/s. Thus, the amplitudes in the R_1 and R_2 frequency ranges, including $\omega_{x0}/N_b =$ 238.52 rad/s and $\omega_{y0}/N_b = 162.17$ rad/s, are the VC primary resonances excited in the *x* and *y* directions of the system, respectively. These two primary resonances exhibit soft spring and soft–hard spring characteristics in the vertical and horizontal directions, respectively, which agrees with previous theoretical and experimental studies [22,24]. Moreover, 1/2-order subharmonic resonances in two degrees of freedom are excited in R_3 and R_4 intervals, where the subharmonic resonant amplitudes are around $2 \cdot \omega_{x0}/N_b = 477.04$ rad/s and $2 \cdot \omega_{y0}/N_b = 324.34$ rad/s.

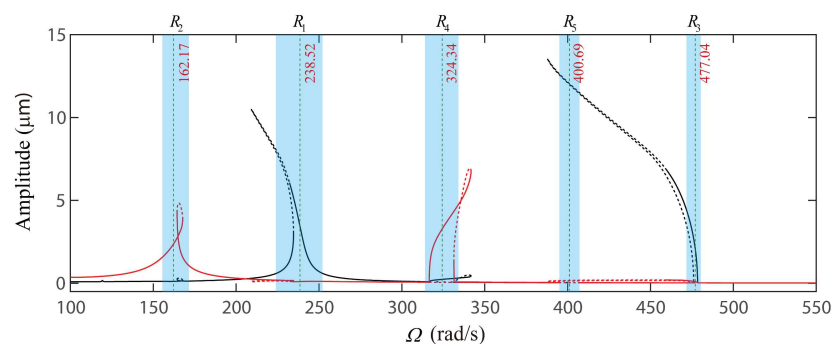**Figure 2.** For $\delta_0 = 1.5$ µm, stable (solid) and unstable (dashed) varying compliance (VC) periodic peak-to-peak frequency–response curves in *x* (red line) and *y* (black line) directions.

As shown in Figure 3a, the resonant amplitude in the R_4 range is excited by supercritical period-doubling bifurcations at points A_1 (see Table 2) and A_2, where the leading Floquet multipliers cross the unit circle at −1. The response characteristics of the period-1 and period-2 motions before and after period-doubling transitions at point A_1 are presented in Figures 4 and 5, and the response amplitude of $y(\tau)$ clearly increases after the bifurcation. Then, the leading Floquet multiplier of the stable VC period-2 solution crosses the +1 axis at A_3 and A_4 (see Table 3), and cyclic fold bifurcation occurs at these two points. This causes significant resonant hysteresis and jumping behaviors in the 1/2-order subharmonic resonance in the horizontal direction. For example, as the control parameter Ω increases, the stable period-2 branch suddenly jumps to the stable period-1 branch from point A_4 to A_5. For the 1/2-order subharmonic resonance as Ω around $2 \cdot \omega_{x0}/N_b = 477.04$ rad/s (i.e., R_3 range), as shown in Figure 3b, supercritical and subcritical period-doubling bifurcations trigger the VC period-2 resonant responses at points B_1 and B_2, respectively. At this time, the subharmonic resonant frequency–response

curve bends to the left, and this soft spring characteristic is consistent with the hysteresis characteristics of the primary resonance in the vertical direction as Ω around $\omega_{x0}/N_b = 238.52$ rad/s.

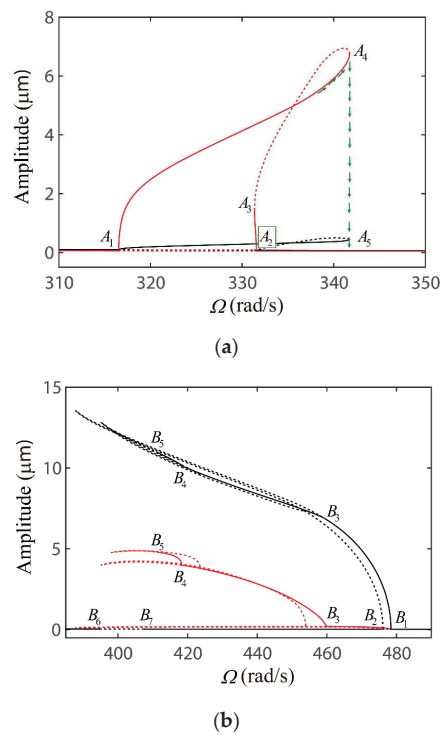**Figure 3.** For $\delta_0 = 1.5$ μm, frequency–response curves of 1/2-order subharmonic resonances of the two degrees-of-freedom of the system, (**a**) in the horizontal and (**b**) vertical directions.
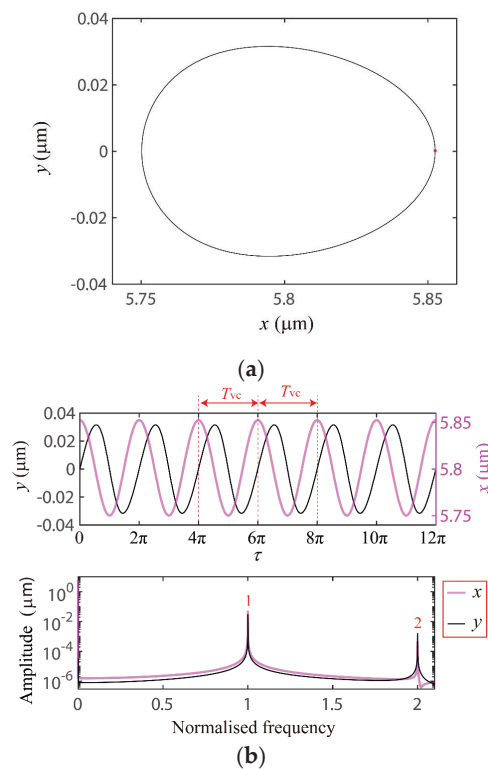

Figure 4. For $\delta_0 = 1.5$ μm, response characteristics of the VC period-1 motion when $\Omega = 310$ rad/s, (**a**) orbit (black line) and its Poincare mapping (red dots), (**b**) time series and their frequency spectra.
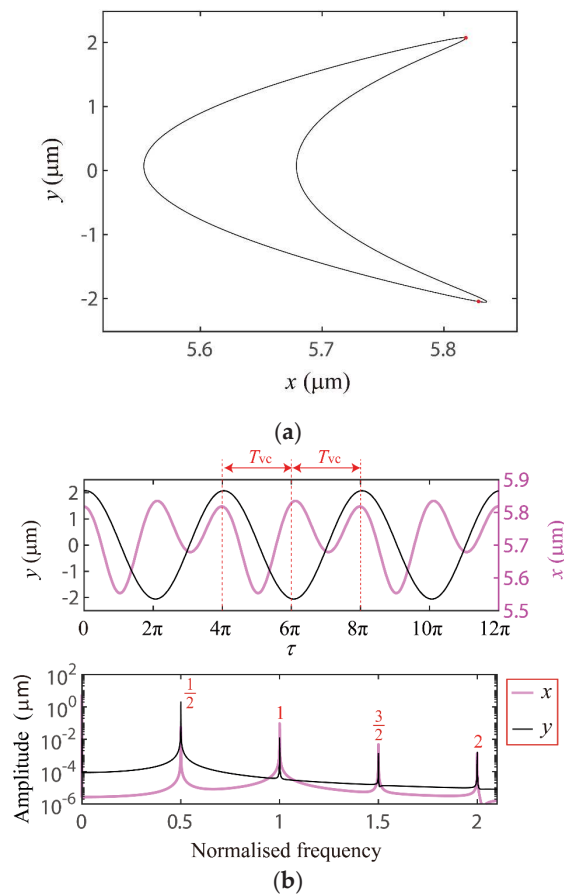
Figure 5. For $\delta_0 = 1.5$ μm, response characteristics of the VC period-2 motion when $\Omega = 330$ rad/s, (**a**) orbit (black line) and its Poincare mapping (red dots), (**b**) time series and their frequency spectra.

Table 2. Period-1 motion Floquet multipliers λ_m around A_1.

Ω	316.3645	316.4645	316.5645	316.6645
λ_m	0.021 + 0.987i	0.019 + 0.987i	0.018 + 0.988i	0.017 + 0.988i
	0.021 − 0.987i	0.019 − 0.987i	0.018 − 0.988i	0.017 − 0.988i
	−0.988 + 0.009i	−0.995	−1.002	−1.006
	−0.988 − 0.009i	−0.980	−0.974	−0.969

Table 3. Period-2 motion Floquet multipliers λ_m around A_4 (counterclockwise, see Figure 3a).

Ω	341.7310	341.7316	341.7316	341.7315
λ_m	−0.536 + 0.817i	−0.535 + 0.818i	−0.535 + 0.818i	−0.535 + 0.818i
	−0.536 − 0.817i	−0.535 − 0.818i	−0.535 − 0.818i	−0.535 − 0.818i
	0.987	0.998	1.001	1.002
	0.968	0.957	0.954	0.953

Moreover, the stable period-2 solution branch undergoes supercritical period-doubling bifurcation at B_3, generating a stable period-4 branch B_3-B_4. Then, a period-8 solution branch B_4-B_5 is excited by supercritical period-doubling bifurcation at point B_4., where point B_5 is the cycle-doubling bifurcation point. In the above bifurcation process, the strongly excited resonant period-2 and period-4 motion modes in the x direction become saturated at B_3 and B_4 points, and the energy spills over into the period-4 and period-8 motion modes in the y direction as Ω decreases, respectively. This typical saturation phenomenon has been discussed in [26,27]. In short, the 1/2-order subharmonic resonances are aroused by the period-doubling bifurcation instability, and they contain complex hysteresis

characteristics. Finally, as shown in Figure 6, the above results agree well with the numerical bifurcation diagrams from the local-maxima method [52].
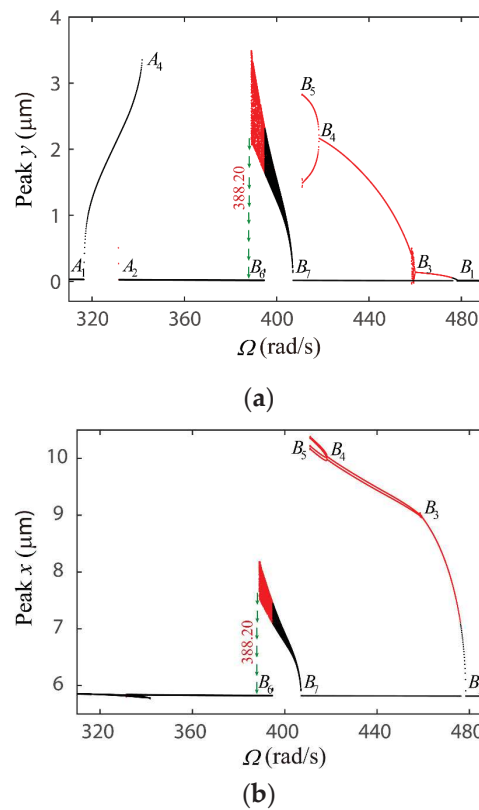

(a)

(b)

Figure 6. For $\delta_0 = 1.5$ µm, numerical bifurcation diagrams of local maxima (**a**) $y(\tau)$ and (**b**) $x(\tau)$ when Ω sweeps up (black dots) and down (red dots).

Furthermore, another resonant amplitude is excited around $\omega_{x0}/N_b + \omega_{y0}/N_b = 400.69$ rad/s (i.e., the resonant range R_5 between intervals R_3 and R_4 presented in Figure 2), and this case of resonance results in strong coupling to the two degrees-of-freedom of the system as shown in Figure 6. In terms of the bifurcation characteristics concerned, as a pair of complex conjugate Floquet multipliers move out of the unit circle (see Table 4), subcritical and supercritical secondary Hopf bifurcations occur at points B_6 and B_7, respectively, leading quasi-period responses excited at point B_7. The response characteristics of the quasi-period motion at $\Omega = 400$ rad/s is presented in Figure 7; as there are incommensurable frequency components, the Poincare mapping of the response orbit tends to a closed point set. Herein, the values of the main incommensurable dimensionless VC frequencies p and q are about 0.5936 and 0.4074, respectively, and p + q = 1, where the value 1 is the dimensionless VC excitation frequency $\Omega_{VC} = N_b \cdot \Omega$. Moreover, for the original time scale, the corresponding main frequency components of the response are $N_b \cdot \Omega \cdot p \approx 1899.52$ rad/s and $N_b \cdot \Omega \cdot q \approx 1303.68$ rad/s, which are close to the predicted equivalent resonant frequencies $\omega_{x0} = 1908.14$ rad/s and $\omega_{y0} = 1297.36$ rad/s of the two degrees-of-freedom of System (5). This indicates that the case of $\omega_{x0} + \omega_{y0} = \Omega_{VC}$ combination resonance (i.e., the 1-order summed type of combination resonance) [39,53] occurs in range R_5, and quasi-period resonant responses are excited. In general, the typical combination resonance of multiple degrees-of-freedom systems often causes quasi-period motions [27,54,55]. Therefore, it can be considered that the combination resonance is one of the physical mechanisms of the generation of VC quasi-period motions in rolling bearing systems. In addition, due to the nonlinearities from Hertzian contact and bearing clearance, this combination resonance has soft hysteresis characteristics, and the quasi-period response jumps to the VC period-1 motion branch as Ω decreases to 388.20 rad/s.

Table 4. Period-1 motion Floquet multipliers λ_m around B_7.

Ω	406.9645	407.0645	407.1645	407.2645
λ_m	−0.018 + 1.031i	−0.019 + 1.006i	−0.019 + 0.971i	−0.066 + 0.923i
	−0.018 − 1.031i	−0.019 − 1.006i	−0.019 − 0.971i	−0.066 − 0.923i
	−0.014 + 0.831i	−0.016 + 0.851i	−0.017 + 0.883i	0.027 + 0.925i
	−0.014 − 0.831i	−0.016 − 0.851i	−0.017 − 0.883i	0.027 − 0.925i

(a)

(b)
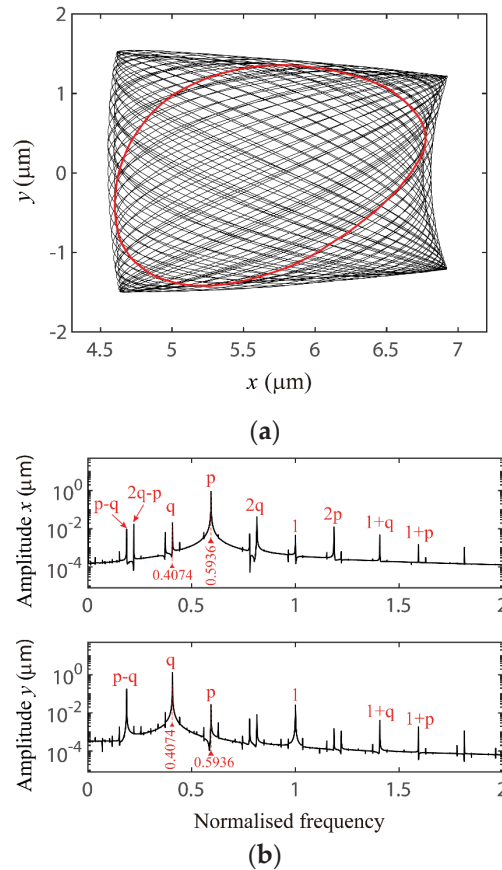
Figure 7. For $\delta_0 = 1.5$ μm, VC quasi-period response characteristics, (**a**) orbit (black line) and its Poincare mapping (red dots), (**b**) frequency spectrum when $\Omega = 400$ rad/s.

For certain applications, such as high-speed or high-precision machines, to increase bearing stiffness and reduce the run-out and noise due to elastic deformation or clearance [11,39], it is possible to eliminate clearance and introduce small interference (negative clearance) in the bearings. Figure 8 presents frequency–response curves of the VC parametric response for $\delta_0 = -1.5$ μm. In this case, the equivalent resonant frequencies of the two degrees-of-freedom of System (5) are about $\omega_{x0} = 1959.49$ rad/s and $\omega_{y0} = 2105.55$ rad/s. Compared to the case of $\delta_0 = 1.5$ μm, the resonant excitation frequency is higher in the horizontal direction than in the vertical direction, and this frequency exchange, due to the adjusting of bearing clearance, was previously illustrated by Fang [56] and Zhang [25], respectively. Herein, the VC primary resonances as Ω rotates around $\omega_{x0}/N_b = 244.94$ rad/s and $\omega_{y0}/N_b = 263.19$ rad/s, 1/2-order subharmonic resonances as Ω rotates around $2 \cdot \omega_{x0}/N_b = 489.88$ rad/s and $2 \cdot \omega_{y0}/N_b = 526.38$ rad/s, and the case of $\omega_{x0} + \omega_{y0} = \Omega_{VC}$ combination resonance as Ω rotates around $\omega_{x0}/N_b + \omega_{y0}/N_b = 508.13$ rad/s are also excited. The difference compared to the case of $\delta_0 = 1.5$ μm is that, as shown in Figure 9, the primary and 1/2-order subharmonic resonances of the system in vertical directions (i.e., the R_1 and R_3 ranges) exhibit soft–hard and hard spring characteristics, respectively, and the bifurcations excited by the combination resonance at the points C_1 and C_2 are all supercritical Hopf types. These bifurcation characteristics are clearly illustrated by the numerical bifurcation diagrams in

Figure 10. In addition, the VC 2-order superharmonic resonances of the two degrees-of-freedom of the system are strongly excited as Ω rotates around $1/2 \cdot \omega_{x0}/N_b = 122.47$ rad/s and $1/2 \cdot \omega_{y0}/N_b = 131.60$ rad/s (i.e., the R_6 and R_7 ranges in Figure 8), respectively. Figure 11 presents the response characteristics of the 2-order superharmonic resonance in the y direction of the system, in which the superharmonic frequency component dominates the period-1 response of $y(\tau)$.
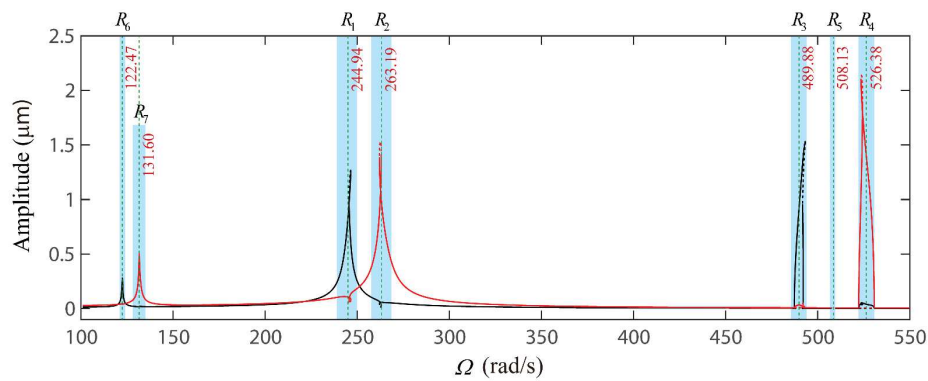
Figure 8. For $\delta_0 = -1.5$ μm, stable (solid) and unstable (dashed) VC periodic peak-to-peak frequency–response curves in x (red line) and y (black line) directions.
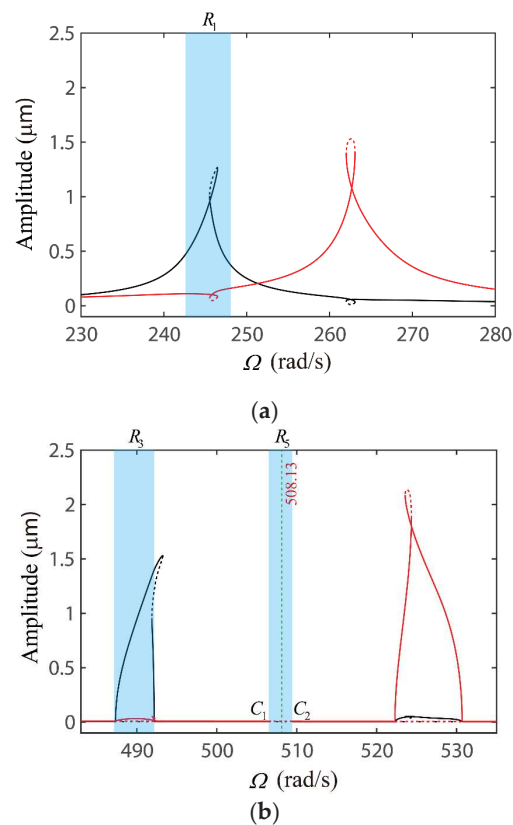
Figure 9. For $\delta_0 = -1.5$ μm, frequency–response curves of (**a**) primary resonances, and (**b**) 1/2-order subharmonic resonances of the two degrees-of-freedom of the system.
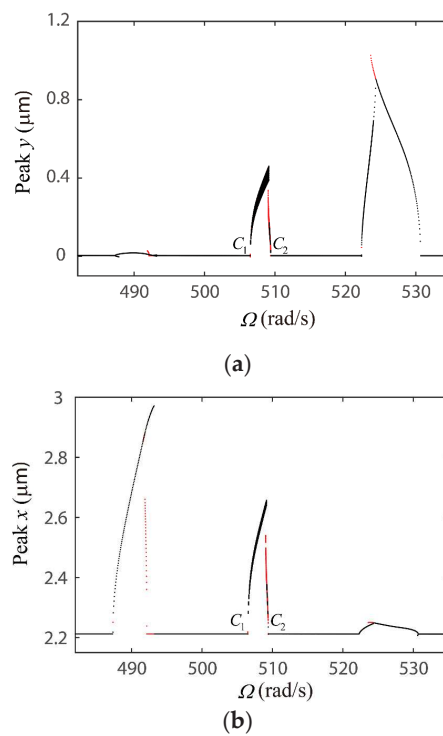
Figure 10. For $\delta_0 = -1.5$ μm, numerical bifurcation diagrams of local-maxima (**a**) $y(\tau)$ and (**b**) $x(\tau)$ when Ω is sweeping up (black dots) and down (red dots).
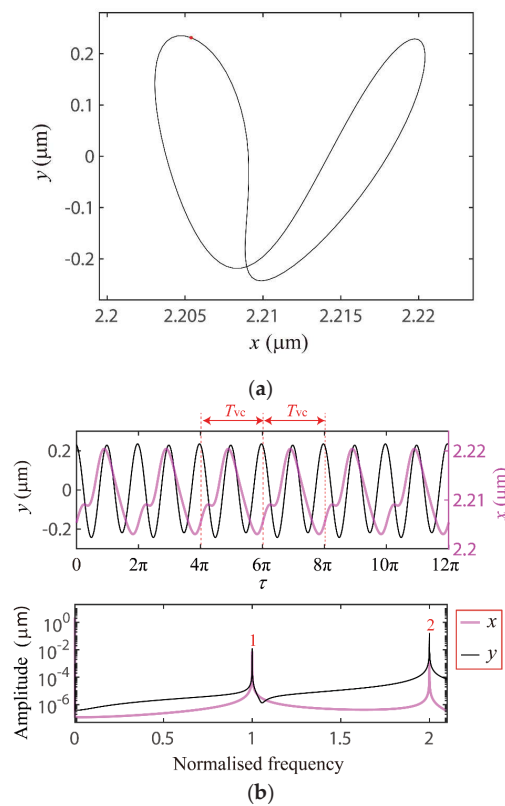
Figure 11. For $\delta_0 = -1.5$ μm, response characteristics of the VC superharmonic motion when $\Omega = 131.6$ rad/s, (**a**) orbit (black line) and its Poincare mapping (red dots), (**b**) time series and their frequency spectra.

4.2. Global Response Characteristics of VC Resonances around the Bearing Clearance-Free Operations

Figure 12 shows the power spectra of the dynamic displacement parameter (*DDP*) [9]: *DDP* = $x_{\text{peak-to-peak}} + y_{\text{peak-to-peak}}$, where $x_{\text{peak-to-peak}} = x(t)_{\max} - x(t)_{\min}$, and $y_{\text{peak-to-peak}} = y(t)_{\max} - y(t)_{\min}$. To reflect the hysteresis characteristics, here the larger *DDP* values are selected from the two *DDP* values obtained as the controlled parameter Ω runs up and down. It is clear that the system contains many types of VC parametric resonances. From Section 4.1, some resonance types of the two degrees-of-freedom of the system have been confirmed, such as the primary resonances (i.e., R_1 and R_2), 1/2-order subharmonic resonances (i.e., R_3 and R_4), 2-order superharmonic resonances (i.e., R_6 and R_7), and the case of $\omega_{x0} + \omega_{y0} = \Omega_{\text{VC}}$ combination resonance (i.e., R_5). Moreover, the cases of $1/2 \cdot (\omega_{x0} + \omega_{y0}) = \Omega_{\text{VC}}$ combination resonance (i.e., the 2-order summed type of combination resonance [39,57]) and $1/2 \cdot (1/4 \cdot \omega_{x0} + \omega_{y0}) = \Omega_{\text{VC}}$ combination resonance (labelled as R_8 and R_9, respectively) were found in our recent work [25]. As shown in Figure 13, these resonant locations can be predicted well by the equivalent resonant frequencies ω_{x0} and ω_{y0} from the arithmetic mean of Equation (8) at $\Omega = 700$ rad/s, where we assume that the system is far from any resonance when Ω takes 700 rad/s to achieve an almost linearized dynamic stiffness (7). In addition, there are the other cases of $1/2 \cdot (1/2 \cdot \omega_{x0} + \omega_{y0}) = \Omega_{\text{VC}}$ and $1/2 \cdot (\omega_{x0} + 1/2 \cdot \omega_{y0}) = \Omega_{\text{VC}}$ combination resonances (labelled as R_{10} and R_{11}, respectively) excited as the bearing clearance δ_0 increases beyond 2.0 μm.
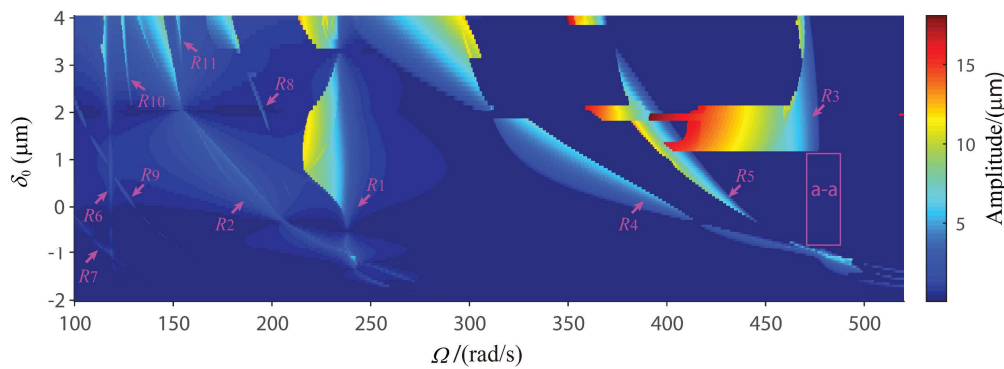

Figure 12. Power spectra of response amplitude around the bearing clearance-free operations.
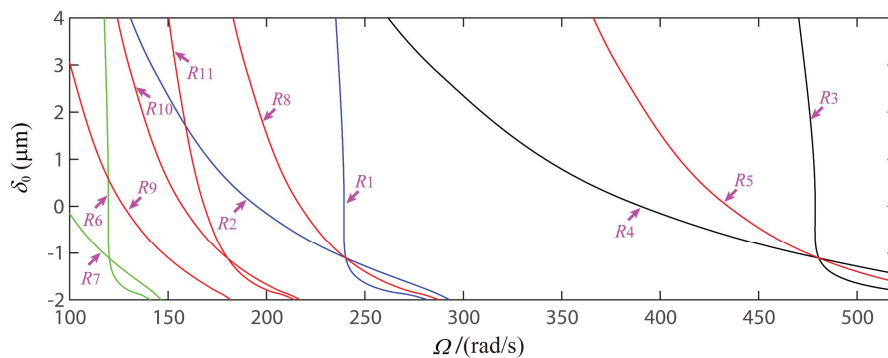

Figure 13. The locations of primary resonances (blue lines), 1/2-order subharmonic resonances (black lines), 2-order superharmonic resonances (green lines), and combination resonances (red lines) predicted by the equivalent resonant frequencies ω_{x0} and ω_{y0}.

As shown in Figures 12 and 13, the equivalent resonant frequency ω_{y0} quickly falls relative to ω_{x0}. This results in the resonant amplitudes R_2 and R_4 shifting to a significantly lower frequency, and the locations of primary resonance R_1 and the 1/2-order subharmonic resonance R_4 to be closer. For $\delta_0 = 4.0$ μm, the equivalent resonant frequencies of the two degrees-of-freedom of System (5) are about $\omega_{x0} = 1881.47$ rad/s and $\omega_{y0} = 1047.21$ rad/s, and the amplitudes of R_1 and R_2 as Ω rotates around $\omega_{x0}/N_b = 235.18$ rad/s and $\omega_{y0}/N_b = 130.90$ rad/s in Figure 14 are the two VC primary resonances,

respectively. Herein, the primary resonance R_1 and the 1/2-order subharmonic resonance R_4 are close to a slight superposition.

The case of $\omega_{x0} + \omega_{y0} = \Omega_{VC}$ combination resonance is triggered from the subcritical and supercritical secondary Hopf bifurcations occurring at points E_5 and E_6, and bends to the left, exhibiting strong soft spring characteristics (see Figure 15). There are abundant quasi-period responses (e.g., see Figure 16), tori doubling (e.g., see Figure 17) [22,51], and even chaotic motion (e.g., see Figure 18) excitements. Moreover, VC period responses such as period-35 and period-8 motions are also excited by this combination resonance as shown in Figures 19 and 20, respectively. Based on the above analysis, it is clear that the VC parametric combination resonance can result in various response types to the system for a bigger bearing clearance δ_0. One reason is that, due to the coupling nonlinearities from the bearing clearance and the Hertzian contact of System (5), the amplitude of the combination resonance strongly bends to the left with a large interval of Ω, and this causes the main frequency components p and q of the response to be modulated significantly, because:

$$N_b \cdot \Omega \cdot \begin{bmatrix} p \\ q \end{bmatrix} \approx \begin{bmatrix} \omega_{x0} \\ \omega_{y0} \end{bmatrix}. \tag{23}$$

Secondly, considering the soft spring characteristics of the combination resonance tail, the equivalent resonant frequencies [ω_{x0}, ω_{y0}] in Equation (23) reduce as Ω sweeps down; for example, as the values of the main frequency components [p q] are [0.6345, 0.3655], [0.6312, 0.3688], [0.6259, 0.3741], [22/35, 13/35], and [5/8, 3/8] when Ω takes 368 rad/s, 363 rad/s, 357 rad/s, 355 rad/s and 353 rad/s (see Figures 16–20), respectively. In addition, [ω_{x0}, ω_{y0}] predicted from Equation (23) becomes smaller gradually, except ω_{y0} at $\Omega = 355$ rad/s (see Table 5). Thirdly, in essence the dynamic stiffness (7) is time-varying and influenced by the response characteristics, so the equivalent resonant frequencies ω_{x0} and ω_{y0} might also fluctuate to some extent. Furthermore, due to the dangerous bifurcation [58] shown at points E_7 and E_8, there are also other complex hysteresis and jumping behaviors in the case of $\omega_{x0} + \omega_{y0} = \Omega_{VC}$ combination resonance.
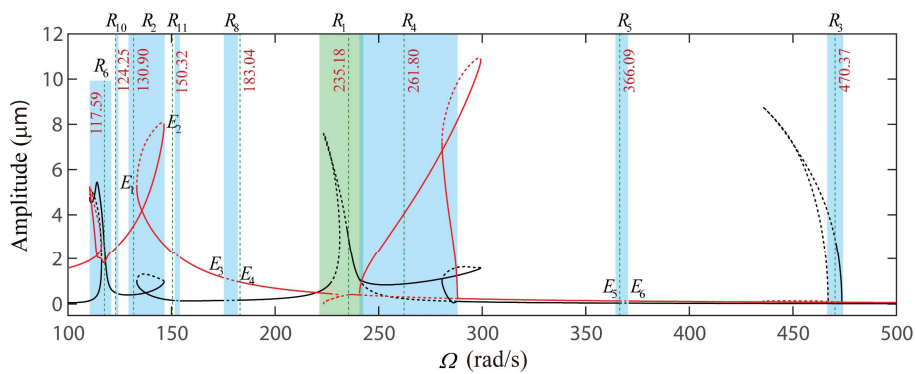

Figure 14. For $\delta_0 = 4.0$ μm, stable (solid) and unstable (dashed) VC periodic peak-to-peak frequency–response curves in x (red line) and y (black line) directions.
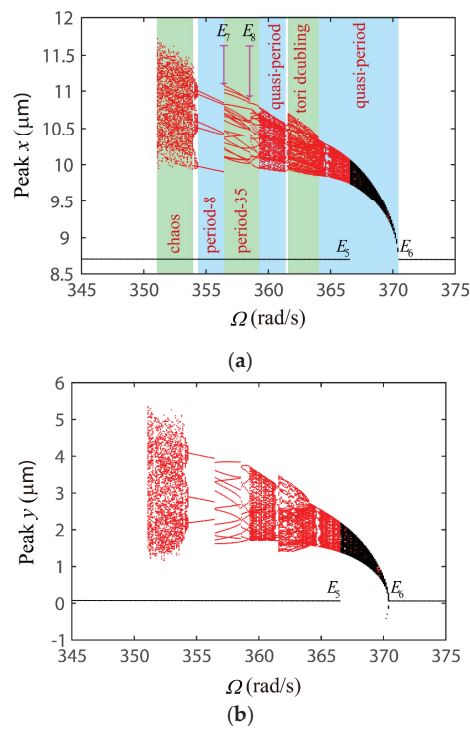
Figure 15. For $\delta_0 = 4.0$ μm, numerical bifurcation diagrams of local maxima (**a**) $x(\tau)$ and (**b**) $y(\tau)$ when Ω sweeps up (black dots) and down (red dots) around 345–375 rad/s.

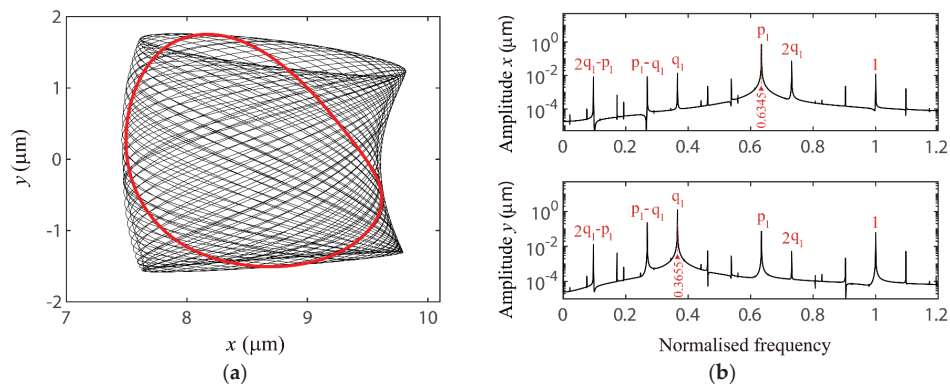**Figure 16.** For $\delta_0 = 4.0$ μm, response characteristics of the VC quasi-period motion when $\Omega = 368$ rad/s, (**a**) orbit (black line) and its Poincare mapping (red dots), (**b**) frequency spectrum.
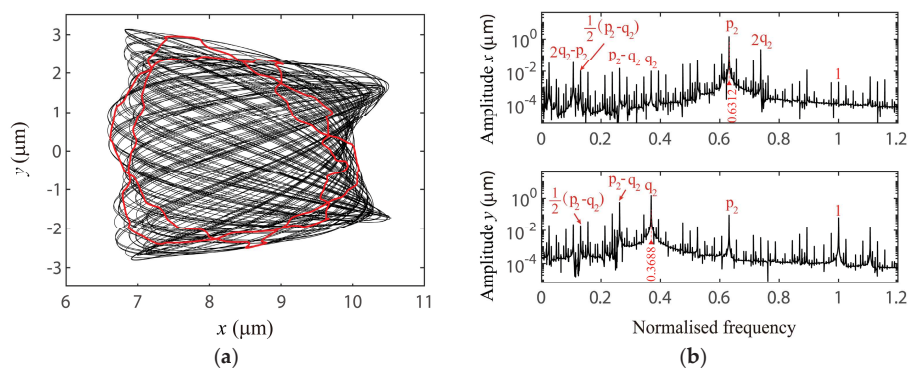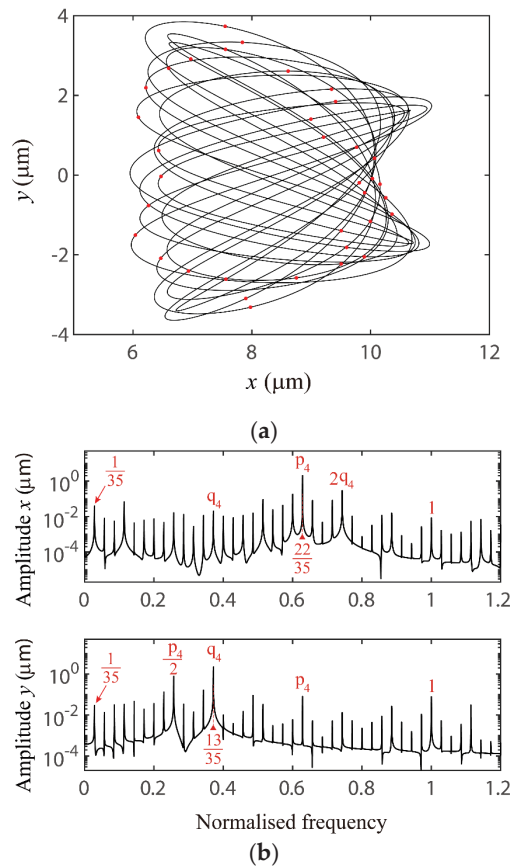

Figure 17. For $\delta_0 = 4.0$ μm, response characteristics of the VC quasi-period motion (the tori-doubling case) when $\Omega = 363$ rad/s, (**a**) orbit (black line) and its Poincare mapping (red dots), (**b**) frequency spectrum.
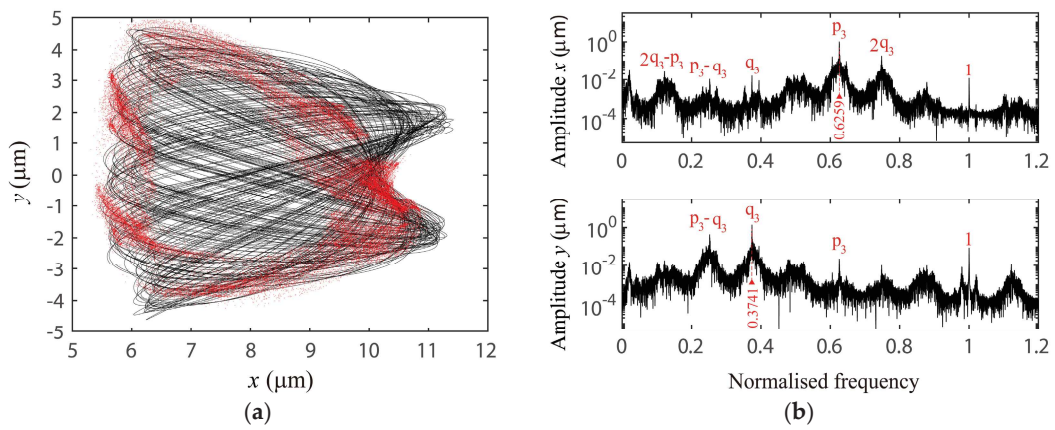
Figure 18. For $\delta_0 = 4.0$ μm, response characteristics of the VC chaotic motion when $\Omega = 353$ rad/s, (**a**) orbit (black line) and its Poincare mapping (red dots), (**b**) frequency spectrum.

Figure 19. For $\delta_0 = 4.0$ μm, response characteristics of the VC period-35 motion when $\Omega = 357$ rad/s, (**a**) orbit (black line) and its Poincare mapping (red dots), (**b**) frequency spectrum.
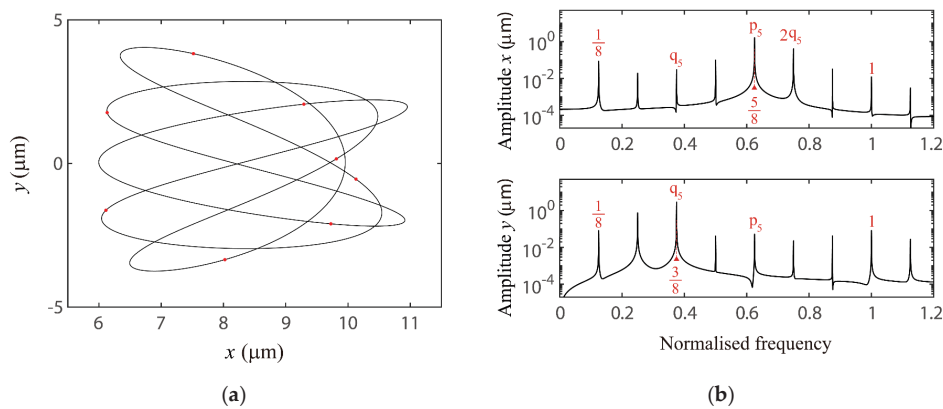
Figure ... ics ... rad/s, (**a**) orbit (black line) and its Poincare mapping (red dots), (**b**) frequency spectrum.

Table 5. The equivalent resonant frequencies of the system predicted from Equation (23).

Ω	353	355	357	363	368
ω_{x0} (rad/s)	1767.54	1775.00	1795.20	1833.00	1867.97
ω_{y0} (rad/s)	1056.46	1065.00	1060.80	1071.00	1076.03

For $\delta_0 = 4.0$ μm, the cases of $1/2 \cdot (\omega_{x0} + \omega_{y0}) = \Omega_{VC}$, $1/2 \cdot (1/2 \cdot \omega_{x0} + \omega_{y0}) = \Omega_{VC}$, and $1/2 \cdot (\omega_{x0} + 1/2 \cdot \omega_{y0}) = \Omega_{VC}$ combination resonances are excited as Ω is close to $1/2 \cdot (\omega_{x0} + \omega_{y0})/N_b = 183.04$ rad/s, $1/2 \cdot (1/2 \cdot \omega_{x0} + \omega_{y0})/N_b = 124.25$ rad/s, and $1/2 \cdot (1/2 \cdot \omega_{x0} + \omega_{y0})/N_b = 150.32$ rad/s (i.e., the R_8, R_{10}, and R_{11} ranges in Figure 14), respectively. The locations of these combination resonances are clearly exhibited by the numerical bifurcation diagrams in Figure 21. Herein, the case of $1/2 \cdot (\omega_{x0} + \omega_{y0}) = \Omega_{VC}$ combination resonance is triggered from the supercritical secondary Hopf bifurcations occurring at points E_3 and E_4, and results in quasi-period (e.g., see Figure 22) and period-4 resonant responses (e.g., see Figure 23) in the system; the main frequency components of the response satisfy $1/2 \cdot (p + q) = 1$, which has been indicated in [25]. Figure 24 shows the quasi-period responses excited in the cases of $1/2 \cdot (1/2 \cdot \omega_{x0} + \omega_{y0}) = \Omega_{VC}$ and $1/2 \cdot (\omega_{x0} + 1/2 \cdot \omega_{y0}) = \Omega_{VC}$ combination resonances, respectively, and there are chaotic motions excited in the case of the $1/2 \cdot (\omega_{x0} + 1/2 \cdot \omega_{y0}) = \Omega_{VC}$ combination resonance as shown in Figure 25. It has been found in a number of studies [5,6,10–16] that the quasi-period motion is a typical characteristic of VC vibrations in rolling bearing systems. However, to date, its physical mechanism has not been given. From above analysis, it is clear that various cases of combination resonances are internal physical mechanisms of excited quasi-period responses.
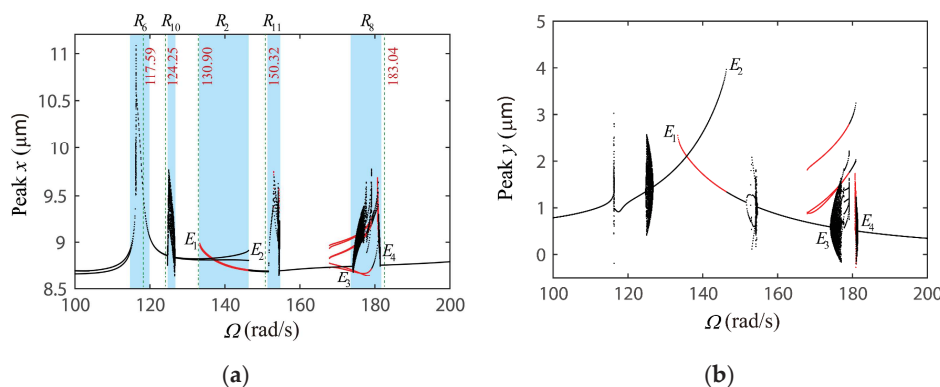

Figure 21. For $\delta_0 = 4.0$ μm, numerical bifurcation diagrams of local maxima (**a**) $x(\tau)$ and (**b**) $y(\tau)$ when Ω sweeps up (black dots) and down (red dots) around 100–200 rad/s.
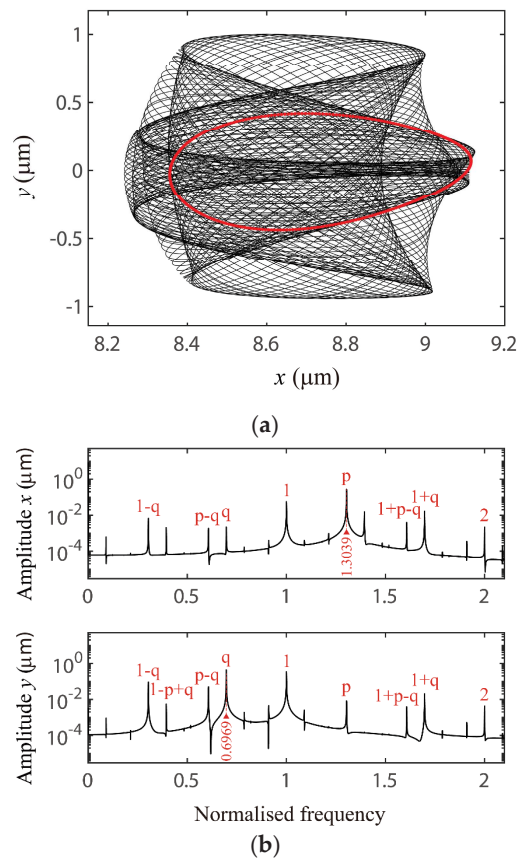
Figure 22. For $\delta_0 = 4.0$ µm, response characteristics of the VC quasi-period motion when $\Omega = 181.2$ rad/s, (**a**) orbit (black line) and its Poincare mapping (red dots), (**b**) frequency spectrum.
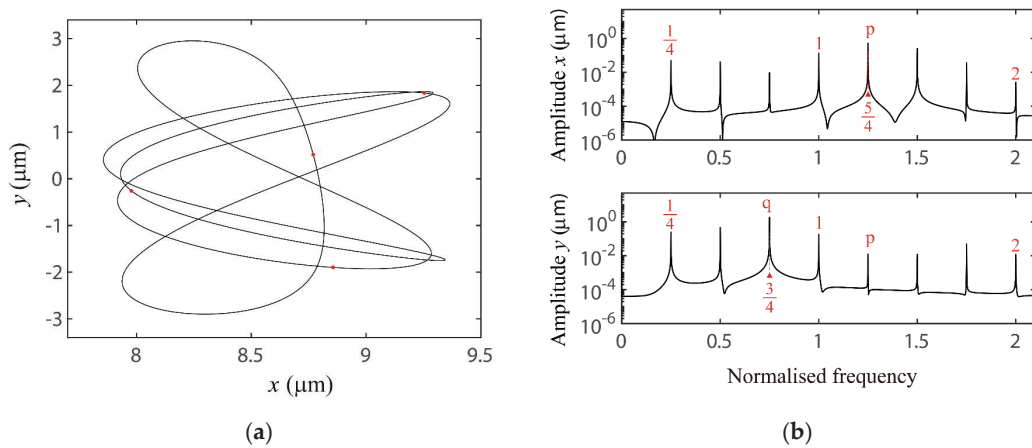

Figure 23. For $\delta_0 = 4.0$ µm, response characteristics of the VC period-4 motion when $\Omega = 180$ rad/s, (**a**) orbit (black line) and its Poincare mapping (red dots), (**b**) frequency spectrum.
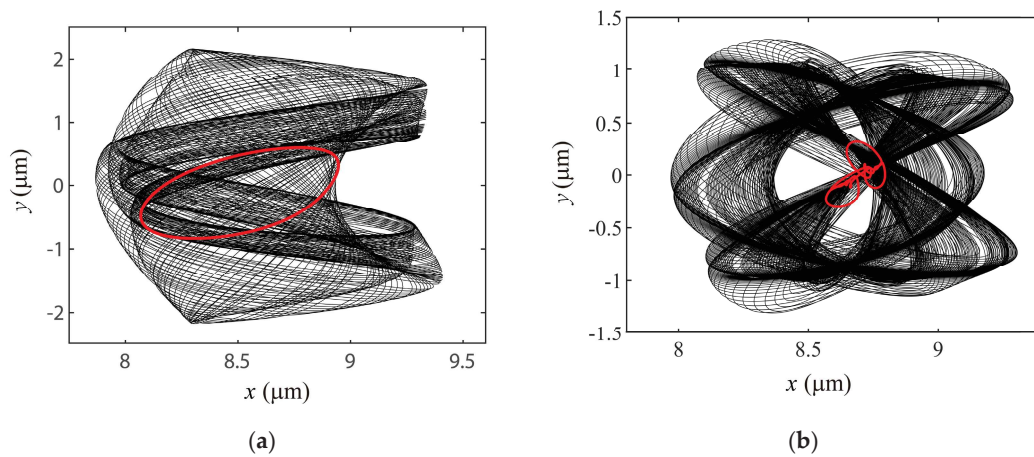
Figure 24. For $\delta_0 = 4.0$ μm, the orbits (black line) and their Poincare mappings (red dots) of the VC quasi-period motion when (**a**) $\Omega = 126$ rad/s, and (**b**) $\Omega = 154.6$ rad/s.
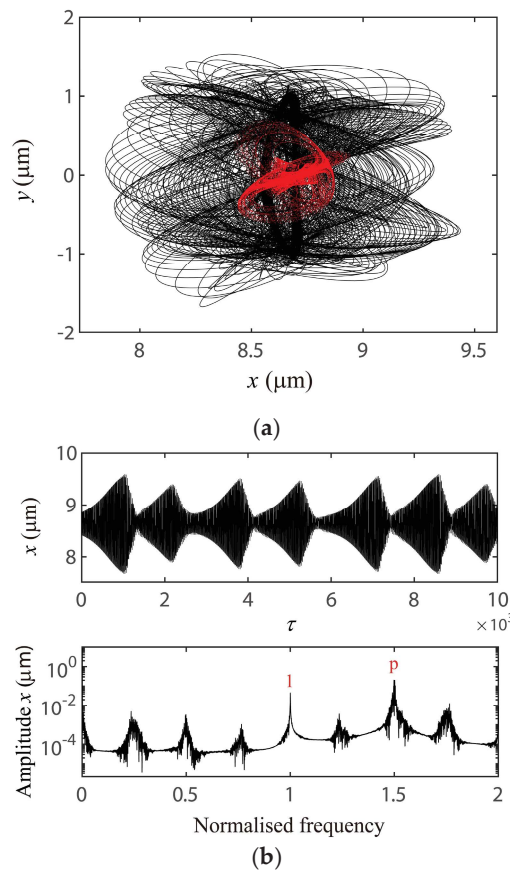

Figure 25. For $\delta_0 = 4.0$ μm, response characteristics of the VC chaotic motion when $\Omega = 154.5$ rad/s, (**a**) orbit (black line) and its Poincare mapping (red dots), (**b**) time series and their frequency spectra.

Comparing Figures 12 and 13, it is clear that not all cases of the predicted VC parametric resonances will be excited; for example, the predicted 1/2-order subharmonic resonance R_3 in the interval a-a. For $\delta_0 = -1.1$ μm, the equivalent resonant frequencies of the system are about $\omega_{x0} = 1921.18$ rad/s and $\omega_{y0} = 1915.54$ rad/s, and only three resonance amplitudes emerge, where the 1/2-order subharmonic resonance is excited by the supercritical period-doubling bifurcations at D_1 and D_2 (see Figures 26 and 27). Therefore, although the rolling bearing is an inherently nonlinear mechanical part [59],

adjusting the bearing clearance may make it operate in a linear range to some extent, and thus avoid some resonances.
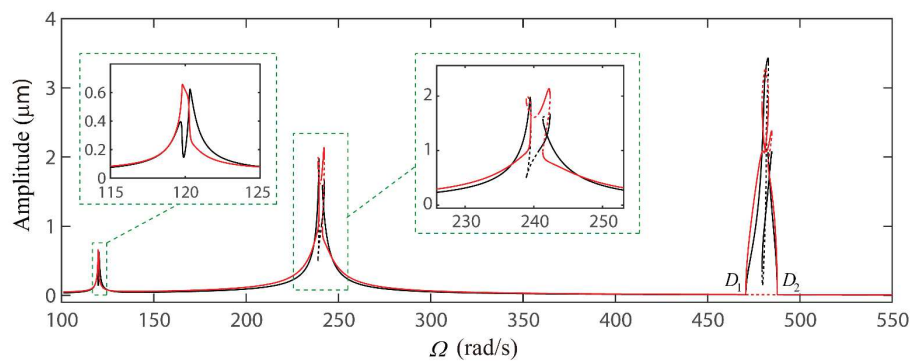

Figure 26. For $\delta_0 = -1.1$ μm, stable (solid) and unstable (dashed) VC periodic peak-to-peak frequency–response curves in x (red line) and y (black line) directions.
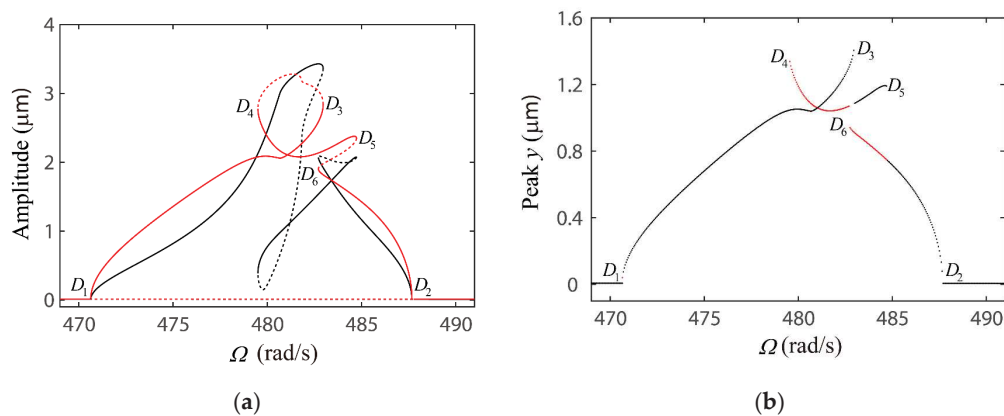

Figure 27. For $\delta_0 = -1.1$ μm, the response characteristics in 1/2-order subharmonic resonance, (**a**) the frequency–response curves in x (red line) and y (black line) directions, and (**b**) numerical bifurcation diagrams of local maxima of $y(\tau)$ when Ω sweeps up (black dots) and down (red dots).

4.3. Discussion on the Verification of Global VC Parametric Resonances

Different from previously works on parametric VC primary resonances, in this paper we extend to study many other parametric VC resonance types such as 1/2-order subharmonic resonances, 2-order superharmonic resonances, and various VC combination resonances. For verification of these new findings, we use our proposed method to reanalyze a classical work from Fukata et al. [14], where they presented that sub/super-harmonic, multi-period, quasi-periodic, and chaos-like motions emerge in System (5). As shown in Table 6, this ball bearing model has a larger bearing clearance $\delta_0 = 20$ μm and a lighter radical load $W = 58.8$ N compared to the above-studied model.

Table 6. Specifications of the ball bearing in [14].

Item	Value
Contact stiffness C_b (N/m$^{3/2}$)	1.334×10^{10}
Ball diameter D_b (mm)	11.9062
Pitch diameter D_h (mm)	52.0
Number of balls N_b	8
Bearing clearance δ_0 (μm)	20
Equivalent mass m (kg)	16
Damping factor c (Ns/m)	2940
Radial load W (N)	58.8

Figure 28 presents frequency–response curves of the VC parametric response of the model in Table 6. In this case, the equivalent resonant frequencies of the model are about ω_{x0} = 1463.75 rad/s and ω_{y0} = 370.74 rad/s. Compared to the case of δ_0 = 4.0 μm in Section 4.2 (i.e., ω_{x0} = 1881.47 rad/s and ω_{y0} = 1047.21 rad/s), the resonant excitation frequencies fall a lot in Fukata's model. Herein, the VC primary resonances as Ω rotates around ω_{x0}/N_b = 182.97 rad/s and ω_{y0}/N_b = 46.34 rad/s are also excited (i.e., the R_1 and R_3 ranges). These two primary resonances exhibit soft spring and soft–hard spring characteristics similar to the case of δ_0 = 4.0 μm studied. Through supercritical and subcritical period-doubling bifurcations trigger at points F_1 and F_2, the 1/2-order subharmonic resonance in the horizontal direction is strong excited in a wide range R_4 as Ω rotates around $2 \cdot \omega_{y0}/N_b$ = 92.68 rad/s, and VC period-2 resonant responses occur. It should be note that 2-order superharmonic resonance in the vertical direction dominates the resonant amplitude R_6 in the vertical direction as Ω rotates around $1/2 \cdot \omega_{x0}/N_b$ = 91.48 rad/s, because the main frequency component of $x(\tau)$ in this range is 2-order harmonics (i.e., the response characteristics at Ω = 88 rad/s presented in Figure 29). Moreover, the period-2 solution branch F_1-F_2 undergoes period-doubling bifurcations at F_3, F_4, F_5 and F_6, generating period-4 branch F_3-F_4 and F_5-F_6. Especially, there are various VC motion types arising subsequently on branch F_5-F_6, including chaotic responses, and this branch contains the beat/chaos-like range b-b described by Fukata et al. [14] (see Figure 30).
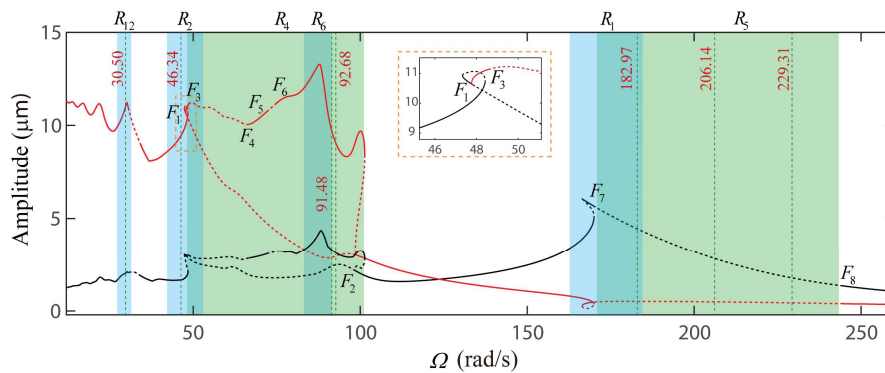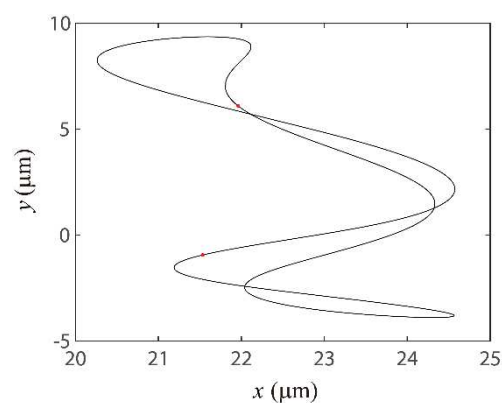

Figure 28. Stable (solid) and unstable (dashed) VC periodic peak-to-peak frequency–response curves in *x* (red line) and *y* (black line) directions.
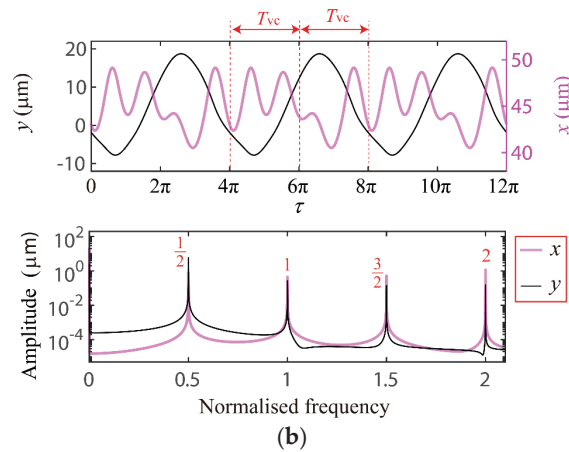

Figure 29. *Cont.*

Figure 29. Response characteristics of the VC period-2 motion when $\Omega = 88$ rad/s, (**a**) orbit (black line) and its Poincare mapping (red dots), (**b**) time series and their frequency spectra.
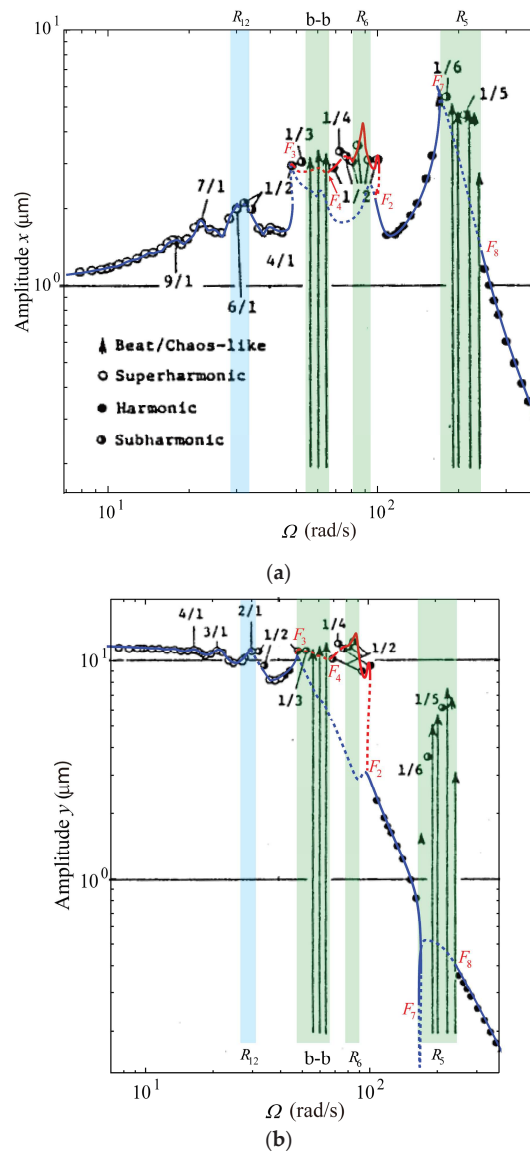

Figure 30. The peak-to-peak frequency–response curves of literature [14] in (**a**) x and (**b**) y directions. Herein, the blue and red lines are the period-1 and period-2 solution branches of Figure 28, respectively, obtained by our work.

Furthermore, the stable period-1 solution branch undergoes supercritical Hopf bifurcations at points F_7 and F_8, and the coming unstable solution branch F_7-F_8 (i.e., R_5 range around $\omega_{x0}/N_b + \omega_{y0}/N_b$ = 229.31 rad/s) contains various VC responses such as period-5, period-6 and beat/chaos-like motions (see Figure 30). The response characteristics of the quasi-period motion as Ω rotates at 242.2277 (i.e., in literature [14], ω_s takes 6000 rpm) are presented in Figure 31. Herein, the values of the main incommensurable dimensionless VC frequencies p and q are about 0.7715 and 0.2285, respectively, and p + q = 1, where the value 1 is the dimensionless VC excitation frequency $\Omega_{VC} = N_b \cdot \Omega$. Moreover, for the original time scale, the corresponding main frequency components of the response are $N_b \cdot \Omega$ $\cdot p \approx 1495.03$ rad/s and $N_b \cdot \Omega \cdot q \approx 442.79$ rad/s, which are close to the predicted equivalent resonant frequencies $\omega_{x0} = 1463.75$ rad/s and $\omega_{y0} = 370.74$ rad/s of the two degrees-of-freedom of System (5). As stated in Section 4.1, this indicates that the case of $\omega_{x0} + \omega_{y0} = \Omega_{VC}$ combination resonance occurs in range R_5. Different from the previous analysis (see Figures 7b and 16b), as shown in Figure 31b, in this case the response–frequency spectrum contains component of 2·q, so there may be the case of $\omega_{x0} + 1/2 \cdot \omega_{y0} = \Omega_{VC}$ combination resonance also excited in R_5, and actually the value $\omega_{x0}/N_b + 1/2 \cdot \omega_{y0}/N_b = 206.14$ rad/s (see Figure 28) is in range R_5. This can explain why the instability range R_5 excited by the combination resonance is so large in Fukata's model. In other words, due to the more asymmetric stiffness characteristics (where $\omega_{x0} = 1463.75$ rad/s and $\omega_{y0} = 370.74$ rad/s), Fukata's model can contain more types of parametric resonances, and these resonances may overlap (literature [27] contains a detailed discussion of this overlapping phenomenon). Due to the vibration mechanism being more complicated, many researchers [44,60] have devoted themselves to investigating the dynamic characteristics of asymmetric rolling bearing-rotor systems. The response characteristics of the period-5 motion as Ω rotates at 211.9492 rad/s (i.e., in literature [14], ω_s takes 5250 rpm) are presented in Figure 32, where its main frequency components p and q are 4/5 and 1/5, respectively; satisfying p + q = 1, and using the above analysis process, it can be found that this period-5 response is also excited by the case of $\omega_{x0} + \omega_{y0} = \Omega_{VC}$ combination resonance. Therefore, the case of $\omega_{x0} + \omega_{y0} = \Omega_{VC}$ combination resonance is the internal mechanism of excitation of various types of VC responses in R_5 range described by Fukata et al. [14] (see Figure 30). In addition, it can be easily verified by our analysis process that the resonant amplitude R_{12} comes from 6-order superharmonic resonance in the vertical direction, because this resonant range emerge as Ω rotates around $1/6 \cdot \omega_{x0}/N_b = 30.50$ rad/s (see Figures 28 and 30). As shown in Figure 33, our above analysis results agree well with the numerical bifurcation diagrams.
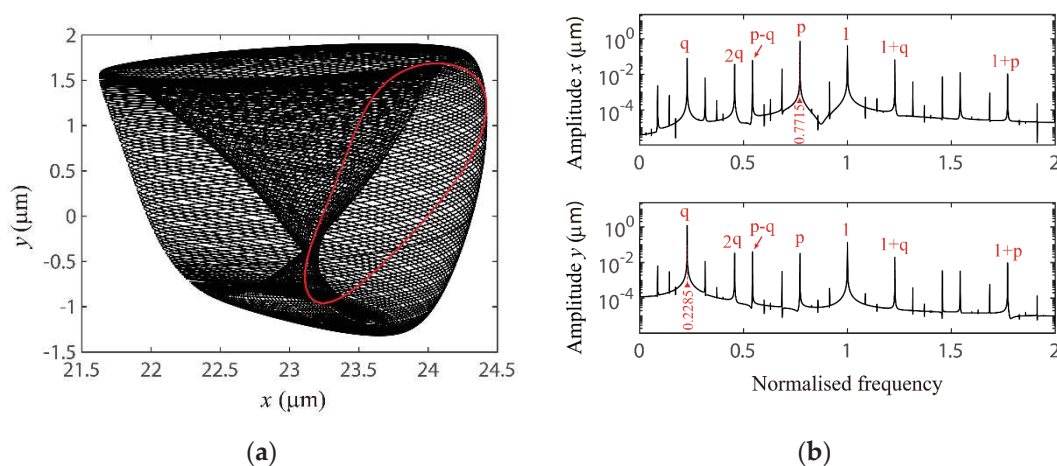

(a)　　　　　　　　　　　　　　　　　　　(b)

Figure 31. Response characteristics of the VC quasi-period motion when Ω = 242.2277 rad/s (i.e., in literature [14], ω_s takes 6000 rpm), (**a**) orbit (black line) and its Poincare mapping (red dots), (**b**) frequency spectrum.
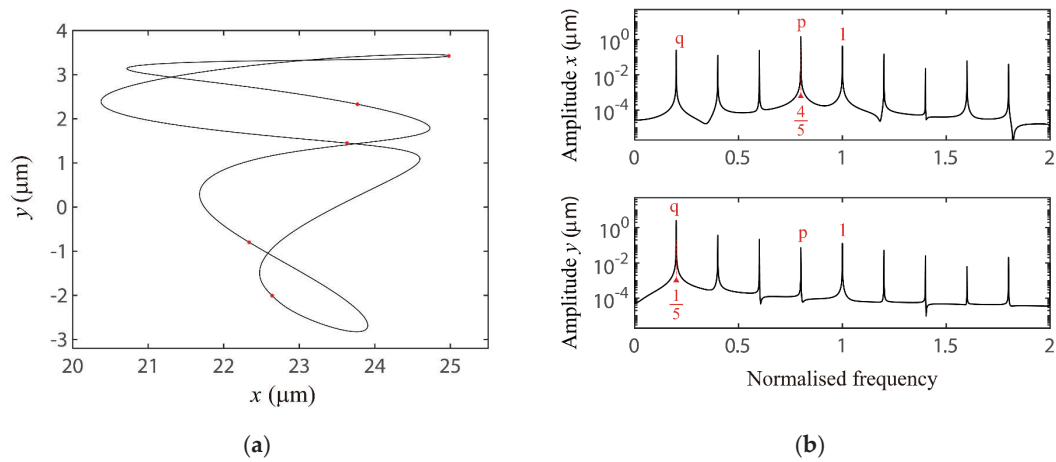
Figure 32. Response characteristics of the VC quasi-period motion when $\Omega = 211.9492$ rad/s (i.e., in literature [14], ω_s takes 5250 rpm), (**a**) orbit (black line) and its Poincare mapping (red dots), (**b**) frequency spectrum.
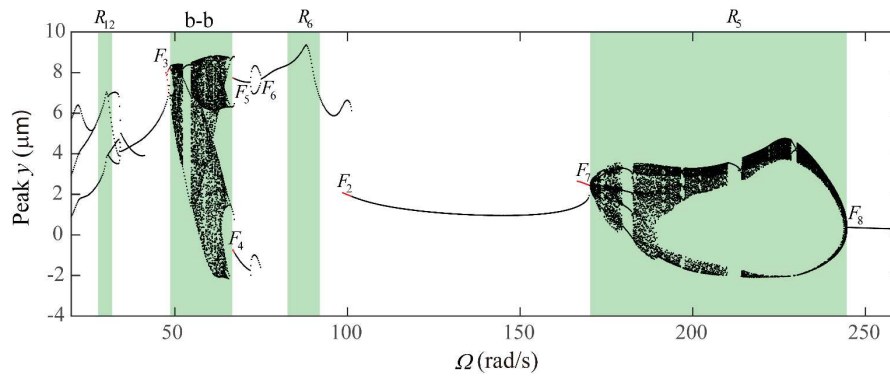

Figure 33. Numerical bifurcation diagrams of local maxima of $y(\tau)$ when Ω sweeps up (black dots) and down (red dots).

For experimental verification, because the VC vibration response is a weak signal, the vibration is usually measured by non-contact displacement sensor in experiments [24,34,61]. The hysteresis characteristics of primary contact resonances have been validated by our previous work [24], and other parametric VC resonances types shown in this paper may be verified in the similar experimental process.

5. Conclusions

In this paper, we investigated the response characteristics of the global VC parametric resonances in a ball bearing system around the bearing clearance-free operations, considering the nonlinearities of bearing clearance and the Hertzian contact between the rolling elements and raceway. The VC period-M motions and their stabilities were traced using the HB–AFT method and Floquet theory. It was shown that the system can contain primary resonances, 1/2-order subharmonic resonances, 2-order superharmonic resonances, and various cases of combination resonances. The 1/2-order VC subharmonic resonances are excited by supercritical/subcritical period-doubling bifurcations, leading to the emergence of VC period-2 motions. Moreover, it was found that the cases of $\omega_{x0} + \omega_{y0} = \Omega_{VC}$, $1/2 \cdot (\omega_{x0} + \omega_{y0}) = \Omega_{VC}$, $1/2 \cdot (1/4 \cdot \omega_{x0} + \omega_{y0}) = \Omega_{VC}$, $1/2 \cdot (1/2 \cdot \omega_{x0} + \omega_{y0}) = \Omega_{VC}$, and $1/2 \cdot (\omega_{x0} + 1/2 \cdot \omega_{y0}) = \Omega_{VC}$ combination resonances can be excited by supercritical/subcritical secondary Hopf bifurcations. Due to the frequency modulation from hysteresis and dynamic stiffness characteristics, the VC parametric combination resonance can result in various VC motion types, such as period-4, period-8, period-35, different cases of quasi-period, and even chaotic responses in the system. Furthermore, it was indicated that the parametric combination resonance is an internal physical mechanism of VC

quasi-period responses trigged in the rolling bearing system. The above results indicate that adjusting the bearing clearance can control the resonant amplitude and its location. Finally, the classical study from Fukata et al. [14] was reanalyzed by our proposed method and the experimental verification of our findings was also discussed. This paper helps clarify the mechanism of complex nonlinear vibration behaviors in rolling bearings.

Author Contributions: Conceptualization, Z.Z.; investigation, Z.Z., Y.Z. and X.L.; methodology, Z.Z.; validation, Z.Z., Y.Z. and X.L.; supervision, T.S. and X.R.; writing—original draft preparation, Z.Z., X.L. and Y.D. All authors have read and agreed to the published version of the manuscript.

Conflicts of Interest: The authors declare no conflict of interest.

References

1. Faraday, M. On a peculiar class of acoustical figures; and on certain forms assumed by groups of particles upon vibrating elastic surfaces. *Philos. Trans. R. Soc.* **1830**, *3*, 49–51.
2. Akhmedov, E.K.; Dighe, A.; Lipari, P.; Smirnov, A.Y. Atmospheric neutrinos at Super-Kamiokande and parametric resonance in neutrino oscillations. *Nucl. Phys. B* **1999**, *542*, 3–30. [CrossRef]
3. Jürgen, B.; Serreau, J. Parametric resonance in quantum field theory. *Phys. Rev. Lett.* **2003**, *91*, 111601.
4. Blocki, W. Ship safety in connection with parametric resonance of the roll. *Int. Shipbuild. Progr.* **1980**, *27*, 36–53. [CrossRef]
5. Di Leonardo, R.; Ruocco, G.; Leach, J.; Padgett, M.J.; Wright, A.J.; Girkin, J.M.; Burnham, D.R.; McGloin, D. Parametric resonance of optically trapped aerosols. *Phys. Rev. Lett.* **2007**, *99*, 010601. [CrossRef] [PubMed]
6. Mei, C.C.; Zhou, X. Parametric resonance of a spherical bubble. *J. Fluid. Mech.* **1991**, *229*, 29–50. [CrossRef]
7. Zhang, W.; Baskaran, R.; Turner, K. Tuning the dynamic behavior of parametric resonance in a micromechanical oscillator. *Appl. Phys. Lett.* **2003**, *82*, 130–132. [CrossRef]
8. Rhoads, J.F.; Shaw, S.W.; Turner, K.L.; Moehlis, J.; DeMartini, B.E.; Zhang, W. Generalized parametric resonance in electrostatically actuated microelectromechanical oscillators. *J. Sound Vib.* **2006**, *296*, 797–829. [CrossRef]
9. Sunnersjö, C.S. Varying compliance vibrations of rolling bearings. *J. Sound Vib.* **1978**, *58*, 363–373. [CrossRef]
10. Qaderi, M.S.; Hosseini, S.A.A.; Zamanian, M. Combination Parametric Resonance of Nonlinear Unbalanced Rotating Shafts. *ASME J. Comput. Nonlinear Dynam.* **2018**, *13*, 111002. [CrossRef]
11. Harnoy, A. *Bearing Design in Machinery: Engineering Tribology and Lubrication*; Marcel D: New York, NY, USA, 2002; pp. 31–33, 431–438.
12. Harris, T.A. *Rolling Bearing Analysis*, 4th ed.; John Wiley & Sons: New York, NY, USA, 2001; pp. 968–980.
13. Lou, J.W.; Luo, T.Y. *Analysis Calculation and Application of Rolling Bearing*; China Machine Press: Beijing, China, 2009; pp. 79–86.
14. Fukata, S.; Gad, E.H.; Kondou, T.; Ayabe, T.; Tamura, H. On the radial vibrations of ball bearings (computer simulation). *Bull. JSME* **1985**, *28*, 899–904. [CrossRef]
15. Mevel, B.; Guyader, J.L. Routes to chaos in ball bearings. *J. Sound Vib.* **1993**, *162*, 471–487. [CrossRef]
16. Mevel, B.; Guyader, J.L. Experiments on routes to chaos in ball bearings. *J. Sound Vib.* **2008**, *318*, 549–564. [CrossRef]
17. Tomović, R.A. Simplified mathematical model for the analysis of varying compliance vibrations of a rolling bearing. *Appl. Sci.* **2020**, *10*, 670. [CrossRef]
18. Sankaravelu, A.; Noah, S.T.; Burger, C.P. Bifurcation and chaos in ball bearings. *ASME Nonlinear Stoch. Dyn.* **1994**, *AMD-192*, 313–325.
19. Ghafari, S.H.; Abdel-Rahman, E.M.; Golnaraghi, F.; Ismail, F. Vibrations of balanced fault-free ball bearings. *J. Sound Vib.* **2010**, *329*, 1332–1347. [CrossRef]

20. Nayak, R. Contact vibrations. *J. Sound Vib.* **1972**, *22*, 297–322. [CrossRef]

21. Hess, D.; Soom, A. Normal vibrations and friction under harmonic loads: Part 1: Hertzian contact. *ASME J. Tribol.* **1991**, *113*, 80–86. [CrossRef]

22. Zhang, Z.Y.; Chen, Y.S.; Cao, Q.J. Bifurcations and hysteresis of varying compliance vibrations in the primary parametric resonance for a ball bearing. *J. Sound Vib.* **2015**, *350*, 171–184. [CrossRef]

23. Zhang, Z.Y.; Chen, Y.S.; Li, Z.G. Influencing factors of the dynamic hysteresis in varying compliance vibrations of a ball bearing. *Sci. China Technol. Sci.* **2015**, *58*, 775–782. [CrossRef]

24. Jin, Y.; Yang, R.; Hou, L.; Chen, Y.; Zhang, Z. Experiments and numerical results for varying compliance contact resonance in a rigid rotor-ball bearing system. *ASME J. Tribol.* **2017**, *139*, 041103. [CrossRef]

25. Zhang, Z.; Sattel, T.; Tan, A.S.; Rui, X.; Yang, S.; Yang, R.; Ying, Y.; Li, X. Suppression of complex hysteretic resonances in varying compliance vibration of a ball bearing. *Shock Vib.* **2020**, *2020*, 8825902. [CrossRef]

26. Zhang, Z.; Rui, X.; Yang, R.; Chen, Y. Control of period-doubling and chaos in varying compliance resonances for a ball bearing. *ASME J. Appl. Mech.* **2020**, *87*, 021005. [CrossRef]

27. Nayfeh, A.H.; Mook, D.T. *Nonlinear Oscillations*; John Wiley & Sons: New York, NY, USA, 1995; pp. 20–26.

28. Tiwari, M.; Gupta, K. Effect of radial internal clearance of a ball bearing on the dynamics of a balanced horizontal rotor. *J. Sound Vib.* **2002**, *38*, 723–756. [CrossRef]

29. Tiwari, M.; Gupta, K.; Prakash, O. Dynamic response of an unbalanced rotor supported on ball bearings. *J. Sound Vib.* **2000**, *238*, 757–779. [CrossRef]

30. Harsha, S.P. Nonlinear dynamic analysis of a high-speed rotor supported by rolling element bearings. *J. Sound Vib.* **2006**, *290*, 65–100. [CrossRef]

31. Upadhyay, S.H.; Haesha, S.P.; Jain, S.C. Analysis of Nonlinear Phenomena in High Speed Ball Bearings due to Radial Clearance and Unbalanced Rotor Effects. *J. Vib. Control* **2010**, *16*, 65–88. [CrossRef]

32. Bai, C.Q.; Xu, Q.Y.; Zhang, X.L. Nonlinear stability of balanced rotor due to effect of ball bearing internal clearance. *Appl. Math. Mech.* **2006**, *27*, 175–186. [CrossRef]

33. Ehrich, F.F. High order subharmonic response of high speed rotors in bearing clearance. *ASME J. Vibr. Acoust.* **1988**, *110*, 9–16. [CrossRef]

34. Yoshida, N.; Takano, T.; Yabuno, H.; Inoue, T.; Ishida, Y. *1/2-Order Subharmonic Resonances in Horizontally Supported Jeffcott Rotor*; IDETC/CIE, ASME: Washington, DC, USA, 2011; Paper No. DETC2011-47605.

35. Bai, C.Q.; Zhang, H.Y.; Xu, Q.Y. Subharmonic resonance of a symmetric ball bearing-rotor system. *Int. J. Non-Linear Mech.* **2013**, *50*, 1–10. [CrossRef]

36. Wu, D.; Han, Q.; Wang, H.; Zhou, Y.; Wei, W.; Wang, H.; Xie, T. Nonlinear dynamic analysis of rotor-bearing-pedestal systems with multiple fit clearances. *IEEE Access* **2020**, *8*, 26715–26725. [CrossRef]

37. Yamamoto, T.A. On the critical speeds of a shaft. *Mem. Fac. Eng. Nagoya Univ.* **1954**, *6*, 160–170.

38. Oswald, F.B.; Zaretsky, E.V.; Poplawski, J.V. Effect of internal clearance on load distribution and life of radially loaded ball and roller bearings. *Tribol. T.* **2012**, *55*, 245–265. [CrossRef]

39. Schaeffler Technologies AG & Co. KG. *The Design of Rolling Bearing Mountings: Design Examples Covering Machines, Vehicles and Equipment*; Fag Bearing company Ltd.: Schweinfurt, Germany, 2012; Publ. No. WL 00 200/5 EA; pp. 11–15.

40. Cameron, T.M.; Griffin, J.H. An alternating frequency/time domain method for calculating the steady state response of nonlinear dynamic systems. *ASME J. Appl. Mech.* **1989**, *56*, 149–154. [CrossRef]

41. Kim, Y.B.; Choi, S.K. A multiple harmonic balance method for the internal resonant vibration of a non-linear Jeffcott rotor. *J. Sound Vib.* **1997**, *208*, 745–761. [CrossRef]

42. Guskov, M.; Thouverez, F. Harmonic balance-based approach for quasi-periodic motions and stability analysis. *ASME J. Vib. Acoust.* **2012**, *134*, 03100335. [CrossRef]

43. Chen, Y.; Rui, X.; Zhang, Z.; Shehzad, A. Improved incremental transfer matrix method for nonlinear rotor-bearing system. *Acta Mech. Sinica-PRC* **2020**, *36*, 1119–1132. [CrossRef]

44. Ehrich, F.F. *Handbook of Rotordynamics*; McGraw-Hill: New York, NY, USA, 1992; pp. 60–116.

45. Adams, M.L. *Rotating Machinery Vibration: From Analysis to Troubleshooting*; Taylor & Francis: New York, NY, USA, 2009; pp. 230–235.

46. Erwin, K. *Dynamics of Rotor and Foundation*; Springer: Berlin, Germany, 1993; pp. 129–138.

47. Teschl, G. *Ordinary Differential Equations and Dynamical Systems*; University of Vienna: Vienna, Austria, 2000; Lecture Notes; pp. 65–76.

48. Chen, Y.S. *Nonlinear Vibrations*; High Education Press: Beijing, China, 2002; pp. 218–231.

49. Li, C.; Qiao, R.; Tang, Q.; Miao, X. Investigation on the vibration and interface state of a thin-walled cylindrical shell with bolted joints considering its bilinear stiffness. *Appl. Acoust.* **2020**, *172*, 107580. [CrossRef]

50. Huang, X.D.; Zeng, Z.G.; Ma, Y.N. *The Theory and Methods for Nonlinear Numerical Analysis*; Wuhan University Press: Wuhan, China, 2004; pp. 79–170.

51. Nayfeh, A.H.; Balachandran, B. *Applied Nonlinear Dynamics*; WILEY-VCH: Weinheim, Germany, 2004; pp. 159–170.

52. Held, G.A.; Jeffries, C.; Haller, E.E. Observation of chaotic behavior in an Electron-hole plasma in Ge. *Phys. Rev. Lett.* **1984**, *52*, 1037–1040. [CrossRef]

53. Yamamoto, T.A. Response curves at the critical speeds of subharmonic and summed and differential harmonic oscillations. *Bull. JSME* **1960**, *3*, 397–403. [CrossRef]

54. Panda, L.N.; Kar, R.C. Nonlinear dynamics of a pipe conveying pulsating fluid with parametric and internal resonances. *Nonlinear Dyn.* **2007**, *49*, 9–30. [CrossRef]

55. Bamadev, S.; Panda, L.N.; Pohit, G. Combination, principal parametric and internal resonances of an accelerating beam under two frequency parametric excitation. *Int. J. Non-Linear Mech.* **2016**, *78*, 35–44.

56. Fang, B.; Wan, S.; Zhang, J.; Hong, J. Research on the influence of clearance variation on the stiffness fluctuation of ball bearing under different operating conditions. *J. Mech. Des.* **2020**, *143*, 023403. [CrossRef]

57. Yamamoto, T.A.; Saito, A. On the vibrations of summed and differential types under parametric excitation. *Mem. Fac. Eng. Nagoya Univ.* **1970**, *22*, 54–123.

58. Thompson, J.M.T.; Stewart, H.B.; Ueda, Y. Safe, explosive, and dangerous bifurcations in dissipative dynamical systems. *Phys. Rev. E.* **1994**, *49*, 1019–1027. [CrossRef]

59. Zhang, Z.Y. Bifurcation and Hysteresis of Varying Compliance Vibrations of a Ball Bearing-Rotor System. Ph.D. Thesis, Harbin Institute of Technology, Harbin, China, 2015.

60. Ishida, Y.; Liu, J.; Inoue, T.; Suzuki, A. Vibrations of an asymmetrical shaft with gravity and nonlinear spring characteristics (isolated resonances and internal resonances). *ASME J. Vib. Acoust.* **2008**, *130*, 38–45. [CrossRef]

61. Yabuno, H.; Kashimura, T.; Inoue, T.; Ishida, Y. Nonlinear normal modes and primary resonance of horizontally supported Jeffcott rotor. *Nonlinear Dyn.* **2011**, *66*, 377–387. [CrossRef]